The effect on lift & drag of an under-wing fire-works launch platform placed near the wingtip.

G.I.R. De Zutter

Technische Universiteit Delft

TU Delft Delft University of Technology

Challenge the future

The effect on lift & drag of an under-wing fireworks launch platform placed near the wingtip.

by

G.I.R. De Zutter

in partial fulfillment of the requirements for the degree of

Master of Science
in Applied Physics

at the Delft University of Technology,
to be defended publicly on Tuesday Februari 2^{nd}, 2024 at 09:30 AM.

Student number:	4220609	
Supervisor:	Prof. Ir. J. A. Melkert	
Thesis committee:	Prof. Dr. Ir. G. La Rocca,	TU Delft
	Prof. Ir. J. A. Melkert,	TU Delft
	Ir. T. J. Mulder,	TU Delft

TU Delft Delft University of Technology

Preface

With this research project my time at the Delft University of Technology comes to an end. I managed to incorporate my hobby as a private pilot in my Master of Science at the faculty of Aerospace Engineering by investigating a real life observation made during the execution of a formation flight. This report investigates this observation and shows the findings on it's merits. I would like to thank a couple of people which where paramount to the completion of this project. First, I'd like to thank my supervisor Joris Melkert who provided me with excellent feedback and insights helping me elevate the scientific value of this project. Secondly I'd like to express my gratitude to my copilots during the test flights. Lisa Tocco, Thibault Claeys, Didier De Booser, Paris Rogiest and Pieter Verbeke did an excellent job in writing down the test values while I executed the testing sequence. Without their help things would have been a lot more difficult. Lastly I can only be grateful for the opportunity and support my parents gave me during my entire study.

G.I.R. De Zutter
Delft, Februari 2024

Abstract

This study investigates the effect on the principal aerodynamic forces caused by home-built under-wing attachments excluding possible consequences on the aircraft's control and manoeuvrability. Many other types of wing attachment have already been used and investigated of time. However, none of these attachments match exactly the attachment under investigation in this study.

For aerial display purposes, one of the team members of the Whiskey Formation Team created an under-wing firework launch platform attached to the tie-down points of the aircraft. These tie-down points are fixed to the quarter chord wing spar at about 90% of the half wing span near the wingtip. The launch platforms themselves protrude about a quarter of their own length in front of the wing's leading edge. The remaining part is attached flush with the wing's lower skin.

After installing the attachments on the aircraft's wing, the creator took it upon himself to do some trial high speed taxi runs followed by a standard take-off. A circuit around the field and a full stop landing completed his trial run during which no adverse effects on the aircraft handling or flight safety could be detected.

Next, on the first trial flight as a formation with the launch platforms attached, the team leader claimed he experienced a slight performance increase. Earlier lift-off and sharper turns were among the examples of this performance increase he gave. No claims on the aircraft's fuel consumption, cruising speed or power-off gliding performance were made. This was not investigated and is deemed not to be relevant to the aerial display.

This report investigates these claims by modelling the aircraft for computational flow simulations, with and without the platforms attached, for both take-off and high G-load turns. For the take-off condition a runway surface is modelled at a wheels-height distance from the aircraft's wing. Realistic speeds of 50 and 60 knots respectively are chosen together with 10 degrees of geometrical pitch.

The result of these simulations was then validated in real life circumstances to eliminate possible adverse results due to modelling error of the real life aircraft. A number of comparative test flights, 5 in total with 6 take-offs per flight, were performed registering weight and take-off speed for a trimmed stick-free configuration. The results obtained from these test flights are likely to confirm the results obtained from the simulations. For the simulations, a larger lift and lower drag force are noted for the configuration with the launch platform attached for The steep turn case. For the take-off case a drag increase was noted. In the real life test this could be confirmed by the almost identical take-off velocities even though this falls well within the error margin of the experimental setup. The gain in lift, most pronounced for the steep turn case, comes from the blocking of the spanwise flow by the launch platforms hereby likely reducing the lift-induced drag caused by the wing tip vortex. The total drag of the modelled wing is reduced for the steep turn case even though the launch platforms contribute to the friction drag. Moreover, the model's lift-to-drag ratio, a common measure of aircraft's performance, is increased.

It can therefore be concluded that for the investigated cases indeed a small effect of the launch platforms on the aircraft's performance can be found though it is deemed unlikely that this difference is be noticeable. Real life tests only show little promise since the error margin occludes the effects on performance. For flight display purposes a different meaning of the word 'performance' is meant. The lift force is considered much more important than the drag force, even though the drag force is reduced too. Therefore it can be concluded that the installation of the launch platforms does not adversely affect the aircraft's performance parameters such as lift and drag. Moreover, it is plausible that they do improve the aircraft's performance parameters and do improve the performance of the aircraft for aerial display purposes.

Contents

List of Figures

List of Tables

Nomenclature

Symbol or accronym	Definition
$AVGASUL91$	Unleaded aviation gasoline 91 octane
$BCAA$	Belgian Civil Aviation Authority
Cl	Lift coefficient
CO_2	Carbon dioxide
F	Normalisation coefficient
kg	Kilogram
$METAR$	Meteorological aerodrome report
μ	Friction force (N)
N	Newton force
P	Pressure ($^N/_{m^2}$
POH	Pilot's operating handbook
ρ	Air density ($^{kg}/_{m^3}$
R_{air}	Air gas constant
S	Wing surface area (m^2)
T	Temperature (K)
V	Airspeed ($^m/_s$)
$VLOF$	Lift-off airspeed
W	Aircraft weight (N)

Table 1: Nomenclature

1

Introduction

While planning for the aerial display on the occasion of the re-opening of the recently renovated clubhouse of Vliegclub Ursel v.z.w., the wingman of the Whiskey Formation Team fabricated two fireworks launch platforms to be attached under each of the aircraft's wings near the wingtips.

The ideal location was found in the tie-down eyes, see Figure 1.1a, which are normally used to secure the aircraft during windy conditions when parked on the apron of an airport or airfield. Two of these eyes are available on the aircraft, one on each wing, making the set-up symmetrical. Structurally, the platforms are attached by metal bolts going through the tie-down eyes and then tightened. Between the wing skin and the upper parts of the platform, an expanding foam mousse is placed both for closing the gap and to create some tension on the bolts to mitigate any possible movement of the platform. From a structural perspective the wingman now deemed the platforms to be safe enough for high speed trials. He was only worried by the aerodynamic consequences the platforms could bring. So, after a high speed taxi on the ground with no sensible adverse effects, the wingman of the formation team took flight for the very first time with the fireworks launch platforms attached. From a legal perspective, the Belgian civil aviation authorities (BCAA) are aware of many fireworks/smoke generating setups and condone the use of them on the pilot's responsibility.

(a) Tie-down eye, attachment point.

(b) Fireworks launch platform

Figure 1.1: Wingtip of the Evektor Sportstar RTC aircraft with launch platform attached.

Before the first flight, a lot of thought went into the structural safety of the platforms. In the event that a fireworks launch platform comes loose on one or both sides of the all-aluminium aircraft, the attachment can either go under or over the wing. If it detaches and goes under the wing, it's proximity to the wingtip and its associated vortex ensures that the path of the detached platform has a spanwise component. This component points spanwise away from the aircraft. Given the proximity of the aileron,

a collision with it can not be ruled out. Since the mass of the platform (0.35 kg) is small and its relative velocity with respect to the wing at the moment of detachment is low, any more damage other than a small dent with an associated scratch on the wing is not to be expected. Given the large spanwise distance of more than two meters between the location of the platforms and the elevator surface, a collision with the elevator is even more unlikely. It is however still possible. In that case, a larger dent and scratch is to be expected. For either the aileron or the elevator it is unlikely that the detached platform would obstruct the proper movement of the control surface. When it detaches and flies over the wing due to the upwash of the air in front of the wing's leading edge, a collision with the aileron is less probable compared to the event that it detaches and goes under the wing. The top surface of the wing itself is expected to show scratches and maybe a small dent. For the elevator, the same minor damage can be assumed if a collision would occur. From Table 3.1 further on this report, one can see that the forces generated by a platform are small. So in the event one of both platforms detaches and an asymmetric situation arises, the force imbalance generated by the remaining platform is not expected to degrade the controllability of the aircraft such that a normal landing would no longer be possible. With these thoughts in mind, the wingman proceeded for a first flight.

During the very first flight, the wingman noticed no harmful effects on the aircraft's manoeuvrability or its control-ability. At a higher altitude, for safety reasons, he performed some stall exercises and incipient spins (No fully developed spins are allowed on this aircraft, but the incipient phase is. [10]) which led him to the same conclusion. Comfortable with the gained insights from the test flight, the team took off for a first formation flight with the launch platforms attached. After that first formation flight, the formation leader, however, indicated that he believes that the fireworks launch platforms are beneficial for the manoeuvres made during the display. This meant for him that the aircraft is more performing due to the launch platforms attached. The meaning he attributes to 'performance' is the ability to make sharper, quicker turns and a more swift take-off. This is a just a specification of the general meaning of aircraft performance used by the Federal Aviation authority: *Performance is a term used to describe the ability of an aircraft to accomplish certain things that make it useful for certain purposes*[11]

The purpose of this report is to investigate the claim of the formation leader on the aircraft's performance by objectively measuring the performance increase or maybe even decrease of the aircraft. Splitting the formation leader's claim in two separate sub-claims lead to the following questions. By attaching the firework launch platforms, is the lift-off speed indeed lowered leading to a sense of swifter take-off? When making sharp turns, is there more centripetal force, i.e. lift, available for the same pitch angle resulting in a smaller turn radius for the same airspeed? Would, for this case, there be more engine power required to overcome the added drag from the launch platforms.

In the next chapter (2) the claim made by the formation leader ,i.e. sharper, quicker turns and faster take-off, is investigated further by defining tests, either analytical, numerical or real-life, to come to a conclusion on whether or not his claim has any measurable merit to it. To be able to investigate the team's leader's claim on the aircraft's performance, relevant literature on the possible aerodynamic consequences of the launch platforms needs to be explored.

Since the early years of aviation many items attached to an aircraft's wing have been used. These with various purposes and their aerodynamic consequences. The next couple of sections each concern a possible type of attachment on the wing along with its use, being either functional, aerodynamic or a combination of these.

1.1. Wing stores

This section interprets the add-ons, perhaps in the closest way to reality possible, i.e. as wing stores. A wing store is an, almost always, under-wing short pylon with an aerodynamically shaped object underneath it. The object often is a rocket or missile, but not exclusively. Bombs and fuel tanks are also examples of other possible objects suspended beneath a wing. They can be seen on many military fighter aircraft. Some examples can be seen in Figures 1.2a and 1.2b

Their use for bomb carriage dates back to the early years of aviation history. The first world war provided the incen-

(a) Under-wing stores of the A10 Warthog [12]

(b) Under-wing stores of the F16 [13]

Figure 1.2: Under-wing stores

tive to develop aircraft able to carry large, heavy and dropable items. This is why, in 1914 at the beginning of the war, the Bréguet 4 bomber aircraft provided an answer to the requirement of the French army to drop explosives behind enemy lines. [14] Initially the contemporary bomber aircraft had their bombs suspended below the fuselage. An example of an aircraft where they are suspended under the wings is the Bréguet 4 as shown in Figure 1.3. From (Żyluk [15]), one knows that from a certain angle of attack a side force on the wing stores exists in the spanwise direction which originates from a certain amount of blocking of the spanwise flow on the underside of the wing. This could already be an initial clue on the possibility that the formation's leader's claims may be valid. Although, the investigated under-wing stores are placed under a swept wing in contrast with the straight wing of the Evektor Sportstar RTC.

1.2. Wing fences

Figure 1.4: Wing fences on the wing of a Sud Aviation SE210 Caravelle [2]

This section explains another type of add-on to reduce the spanwise flow to a minimum thus reducing the induced drag due to the tip vortices caused by this flow. Also known as potential fences or boundary layer fences, wing fences are fixed aerodynamic tools on an aircraft's wing.

Typically wrapping around the wing's leading edge (see Image 1.4) in the direction of flight, the flat plates are often used on swept wings. Preventing the advent of wing stall over the entire wing, by limiting the spanwise flow. Wingtip devices on the other hand improve the aerodynamic efficiency of the wing by recovering parts of the wing vortex energy. When approaching the aircraft's stall speed, the sweep angle of the leading edge promulgates spanwise flow towards the tip from the lower side of the aircraft's wing. See Figure 1.5 This spanwise flow is composed of multiple causes. The flow near the middle of the wing is not only affected by the spanwise flow due to the leading edge, called 'leading edge vortexing', but also by the spanwise flow coming from the wing root. [16] As opposed to the wing root, the flow near the wing tip can become almost fully spanwise such that the effective airspeed drops well below the airfoils stall speed for the angle of attack. From a geometrical point of view, the aft placed wingtips are generally positioned aft the aircraft's centre of gravity thus the lift they generate promotes a nose down pitching moment. However, when they stall, the lift they produce as well as the pitching moment they provide rapidly diminish. This leaves the previously balanced aircraft in an unbalanced state due to the loss of the pitch down moment the wingtips create. This results in an acute and strong pitch-up which is followed by a fully developed stall. For a pilot this situation is difficult to

recover from.[17] By delaying or even eliminating the spanwise flow from moving too fast along the wing, the pitch-up effect is restored and stall characteristics are improved.

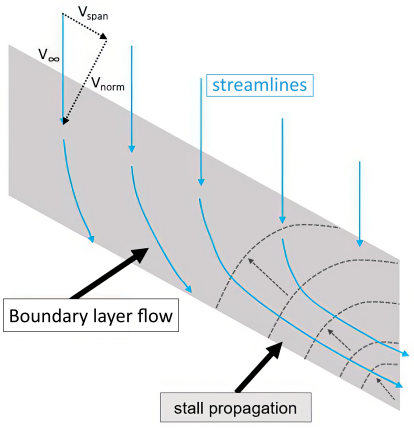

Figure 1.5: Spanwise boundary layer flow [3]

1.3. Vortilons

From the previous section, one knows that fixing a plate on top of the wing has an effect on the spanwise flow. This section describes what would happen if one were to fix a plate-like element to the bottom side of the wing. The origin of the vortilon[18] dates back to the development of the Douglas DC-9 aircraft. It was invented by aerodynamicists working at Douglas Aircraft. After having developed the engine pylons for the DC-8, which originally wrapped the entire leading edge of the wing, they had to cut back the size of the pylons due to the cruise drag becoming too high.[19] During wind tunnel testing for the new aircraft they were designing featuring fuselage mounted engines, they found that a cutback engine pylon on the wing was beneficial for the upwash at the tail and the wing lift at the low speed stall. See Figure 1.6. The pylon thus was called the vortilon.[20] See Figure 1.7.

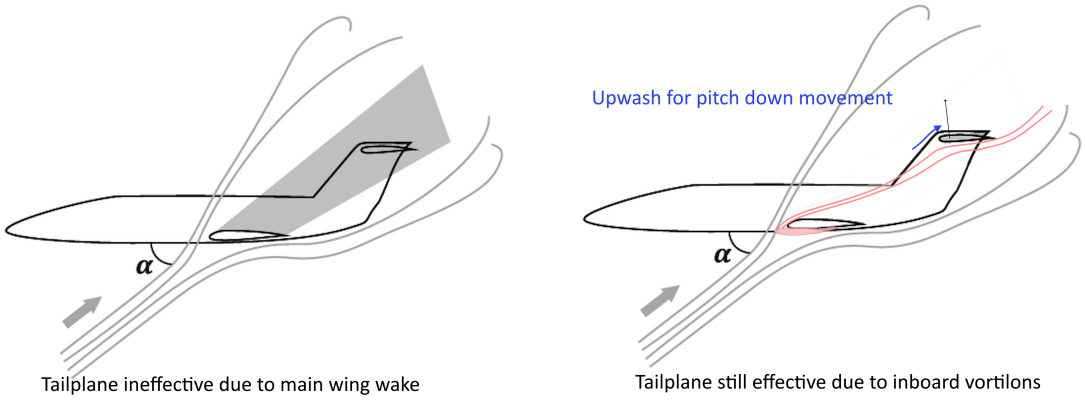

Figure 1.6: Vortilon effect on aircraft elevator

As mentioned before, vortilons were first used for the DC-9 aircraft. This was to introduce a strong nose down pitching moment when going beyond the normal stall angle. However, this ceased to have any effect beyond 30 degrees angle of attack.[19] A vortilon is made up by attaching one or more flat plates on the underside of the wing leading edge, aligned with the flight direction. When approaching the aircraft's stall speed, the local flow around the leading edge points towards the wing tip. This spanwise flow, being partially obstructed by the vortilon becomes rotational and forms a vortex on the upper side of the wing.

This vortex on the upper surface re-energises the boundary layer. This now turbulent boundary layer delays the separation of the local flow. Often used to improve the low-speed performance of the aircraft's ailerons, it also increases its resistance to spin. As an alternative to wing fences they can also be used to restrict the spanwise flow. Vortilons, however, only produce these vortices at high angles of attack and produce less drag at higher velocities as compared to wing fences.[21] However, according to Burt Rutan, the spanwise flow at high angles of attack as observed swept wings, is an essential requirement for vortilons to be effective. On straight wings, he states that vortilons aligned with the flow would not have any effect. [22]

Figure 1.7: Detail view of vortilons [4]

1.4. Wing pylons

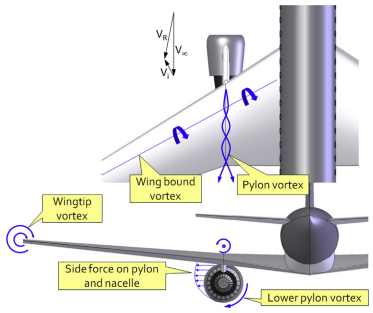

Figure 1.8: Aerodynamics of a wing pylon [5]

This section views the launch platform as a functional item with added aerodynamic benefits, rather than purely aerodynamic. Allegedly, already in the late 40's by Boeing during the development of the B-47 Stratojet, the effect of the wing pylon was discovered.[23] Although common on swept-wing aircraft of that era to have wing fences, the Boeing 707 and B-52 Stratofortress instead featured two pylons per wing to improve the stall characteristics of both jets. As mentioned before, side-wash is induced on the engine pylon by the bound vortex on the wing. This can be seen in Figure 1.8. A side force pointing outwards is generated on the nacelle and the pylon itself. The pylon then generates a vortex opposing the outboard span-wise flow due to its flow direction over the upper surface of the wing. Due to this vortex, early wingtip flow separation is suppressed.

1.5. Winglets

This section reviews several types of aircraft winglets. At present, they have become a key aspect of newly designed aircraft. Besides their aesthetic appeal, they reduce the strength of the wingtip vortex hereby lowering the lift-induced drag.

1.5.1. Whitcomb type

The origin of winglets dates back to the seventies in which an American aeronautical engineer working for NACA, nowadays NASA, called Richard T. Whitcomb introduced a new wingtip design consisting of two plates. A large upper plate and a smaller lower one. See Figure 1.9. He claimed the new wingtip decreases the induced drag by up to 20% alongside an increase in wing lift-to-drag ratio of 6%. All of this while not considerably increasing the wing's bending moment when compared to the other wingtip designs he tested. [24]

Figure 1.9: Whitcomb style winglet [6]

1.5.2. Canted type

Figure 1.10: Canted winglet [7]

By the 1980's, Boeing engineers introduced the canted winglet in an effort to extend the range and loading capacity of their 747-400 freighters and airliners. Much of the increase in lift-to-drag ratio is found to be due to the increase in effective span. Wind-tunnel experiments suggested an increase of 9% though the actual resulting improvement was found to be just about a 4% increase in lift-to-drag ratio. It was observed that the cant angle, i.e. the angle between the wing plane and the plane of the winglet, is not to be decreased too much as the wing properties at larger angles of attach would be affected too much. This is because flow separation will occur more rapidly as the cant angle becomes too small. Stronger vortices are consequently shed from the wing's tip section thus hereby reducing the winglet's efficiency. [25]

1.5.3. Fenced type

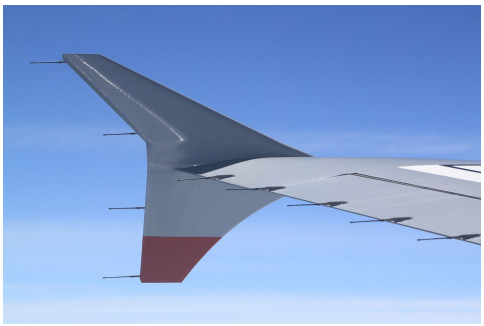

Figure 1.11: Fenced style winglet [8]

In response to its American competitor's canted winglet design, Airbus came up with the fenced winglet also to improve the mileage of their aircraft. In contrast with the canted design, the fenced winglet protrudes both upwards and downwards quasi perpendicular to the wing. The name 'Fenced type' comes from the triangular fence-looking shape. When compared to the lift-to-drag ratio of the clean wing, the in general smaller geometry of the fence type winglet compared to the geometry of other winglet types results in a drag reduction of just about 1.5 - 5 % in cruise. On the other hand, the corresponding increase in wing bending moment, due to the increase in lift of the tip portion of the wing and the inwards load it produces when diverting the tip vortex, is also less prominent due to the smaller size of the winglet type. [26, 27].

1.5.4. Split type

Figure 1.12: Split type winglet on a b737-MAX ©Boeing

Appearing like a Whitcomb style winglet, the next winglet type, the split-tip is a more advanced type due to the difference in size ratio of the upper and lower plate. The best known use of this type of winglet is the Boeing 737 MAX, more specifically named the Boeing 737 Max AT by the company itself. The 'AT' stands for advanced technology and it was announced in 2012.[28] Claims are made that the split-tip, compared to existing blended wingtips, improves the cruise performance by as much as 40%. Furthermore a drag reduction of up to 9.5% compared to an unmodified wing and a reduction of fuel burn of about 1.5% is estimated.[29]

1.5.5. Blended type

(a) Blended winglet on a Boeing 737 [30]

(b) Blended 'Sharklet' winglet on an Airbus A350 XWB [31]

Figure 1.13: Blended winglet types

Just like the canted winglet, the blended winglet consists of an upward swept extension of the wing. Unlike the canted version, the transition now features a smooth chord and angle changes from the wing to the wingtip. Even for non-optimised designs of this type of winglet, a considerable improvement of up to 9% in lift-to-drag ratio can be seen.[32] Initially this design was investigated by Boeing in the 80's to be further developed by Aviation Partners in the early 90's. Available on the Boeing 737-, 757- and 767-series, see Figure 1.13a it was a standard option for the Boeing Business Jet series. A decrease of fuel consumption of about 4-5% has been claimed by Boeing. [33] Airbus answered Boeing's design with the 'Sharklet'. See Figure 1.13b It also offers the same smooth transition in angle and chord and due to its resemblance to a shark fin it adopted the name Sharklet. Launched in 2013 as a retrofit for

the A320 series, it claimed fuel burn decreases of up to 3.4% resulting a a considerable amount of CO_2 emissions saved annually. Moreover, by adding the sharklet wingtip, more lift is generated which allows for a larger payload to be loaded. [34]

1.5.6. Spiroid type

In 1992 Louis B. Gratzer designed an exotic type of winglet called the 'spiroid'. He claimed superior performance in reducing the lift-induced drag. [35] When correctly designed the tip vortices can be reduced considerably. There are two vortex cores formed instead of just one. The low pressure regions at the bends of the spiroid can combine to a single vortex. This vortex now follows a straight path behind the wing. This single vortex does not negatively interact with other parts of the fuselage so an improvement of the aircraft's range is to be expected.[36] The spiral design was first fitted and tested on a Gulfstream II back in 1993 and later on refined and fitted on the Falcon 50 in 2010. Aviation Partners Inc are continuing the development and testing the design for implementation on a wide variety of jet aircraft.[37]

Figure 1.14: Spiroid winglets on a Falcon 50[9]

As stated in the beginning of this chapter, the next Chapter (2) investigates the claim made by the formation leader. In other words, it describes the methods used for the investigation of two well defined plausible cases for which a beneficial effect might be possible. In the third Chapter 3 the results of the investigation are stated and discussed. The last Chapter 4 gives perspective on how the claim of the team's leader could be interpreted and draws a conclusion on the aerodynamic effects due to the fireworks launch platforms under the investigated circumstances.

2

Aerodynamic investigation

This chapter describes how the team leader's claim is investigated. His claim entails two separate occasions where a performance benefit due to the launch platforms is noticed. The first occasion was during the take-off phase that he felt an earlier lift-off with the platforms attached as compared to the clean aircraft. The second occasion is a more general statement. He states that due to the platforms the aircraft can make sharper, quicker turns. Since the manoeuvres are made during a flight display, a realistic occasion where the behaviour of the platforms might be beneficial is during the execution of a steep turn. This chapter begins with the definition of two cases to be examined given the information gathered in the previous chapter. The next section (2.2) defines the implementation of the two cases for computational fluid dynamic (CFD) computations. The third section (2.3) prescribes the test flights used for the result verification of the computations, together with the assumptions made and expected errors on the test results. The last section (2.4 defines how the results obtained from the flight testing are processed and consequently normalised to allow for result comparison when possible.

2.1. Investigated case descriptions

This section clarifies the two situations where a gain in performance could be present as indicated by the team leader considering the information gathered in the first chapter (1) of this report. The two cases under investigation are the 'take-off case' and the 'steep turn' case. From Chapter 1 one knows that many of the add-on's show their benefit at moderate to large angles of attack where they either reduce the spanwise flow of a swept wing or reduce the strength of the wingtip vortex resulting in the lift-induced drag. Since some of the attachments also delay the advent of stall by generating vortices over the wing to re-energise the airflow, low airspeed should also be an element of the cases. The two situations the team leader described, during which he noticed a benefit of the platforms, both entail the two previously mentioned elements of a large angle-of-attack and a low airspeed. One of the aspects not present in these two cases is the spanwise flow due to the sweep, since the aircraft is straight winged. Nonetheless there is spanwise flow over the wing present. This is because the wing is of finite span. When lift is produced one knows that a pressure difference exists between the upper side and lower side of the wing. The lower pressure side is the upper side of the wing. This difference must equal out at the wingtip of the finite wing. This results in spanwise pressure gradients forcing the flow on the lower side of the wing to deflect outwards towards the tip. On the upper side of the wing the opposite is true where the flow is deflected inwards toward the wing root. This can be seen in Figure 2.1. At the trailing edge, where the upper and lower flow over the airfoil meet again, there is a surface of discontinuity formed and a sheet of vortices is

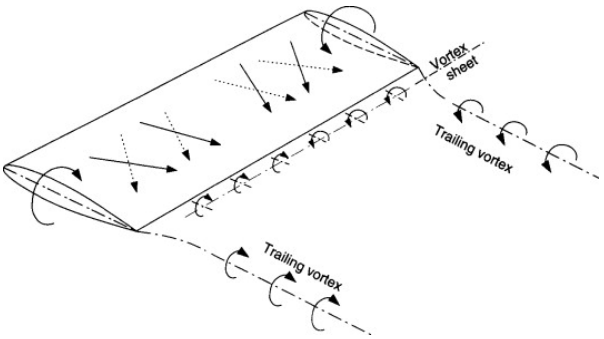

Figure 2.1: Vortex system with indication of spanwise flow over a rectangular wing

created. See Figure 2.2. This sheet of unstable vortices rolls up near the wingtip to form the trailing vortex. [38]

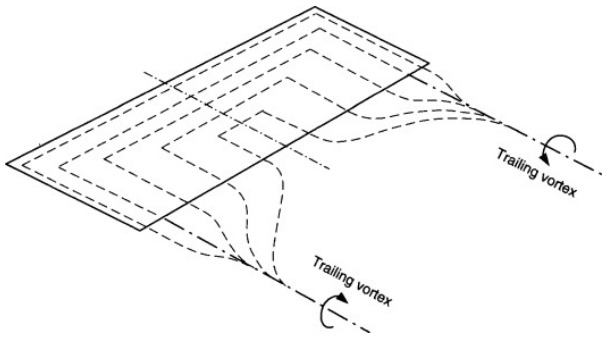

Figure 2.2: Vortex sheet roll up with trailing tip vortices.

The following subsections 2.1.1 and 2.1.2 each describe the circumstances of the case and why the case may be able to prove the statement made by the team leader.

2.1.1. Take-off case

The first test case that will be investigated is the take-off case. This case contains some of the elements such as high angle of attack and low air speeds, as found in literature. Moreover is the nearby presence of the ground also of interest because the ground is known to improve the lifting capability of the aircraft by blocking the spanwise flow from going from the bottom of the wing to the top via the wingtip thus inducing a tip vortex. [39] It is known from the previous chapter (1) that reducing this tip vortex improves the lift-to-drag ratio of the aircraft.

2.1.2. Steep turn case

The second test case, the steep turn case, shares the elements of high angle of attack and low air speeds with the previous case. (2.1.1) In this case, however, there is no ground nearby to block the spanwise flow over the bottom part of the wing. The blocking, if found, would be only due to the firework launch platform. The blocking can be established by measuring the side force on the firework launch platform. From Buler *et al.* [40] it is known for a side force to exist and its influence on the aircraft.

2.2. CFD case analyses

The following section reveals the work-out method used for these two cases to be converted into models suitable for computational fluid dynamic (CFD) computations. First, a suitable model of the wing is made using the line drawing, Figure 2.3, and geometrical data of the aircraft as provided in the pilot's operating handbook.[41] More detailed measurements were made from the actual aircraft stationed at the Ursel Air Base (EBUL) in the town of Aalter, Belgium. The airfoil used for this aircraft is the NACA 2315 mod[42], which is the same airfoil as used for the ultralight version of this aircraft, the Eurostar EV97. The '...mod' denominates the modification made to the base NACA 2315 to close the trailing edge with a double tangent circular arc. Figure A.2 shows the airfoil with the modification indicated. The model consists of the wing only as no interaction effects with e.g. propeller, landing gear, tail surfaces of fuselage are being examined. The reason behind this being that the CFD analysis is used merely to determine the effects of the launch platform on the wing.

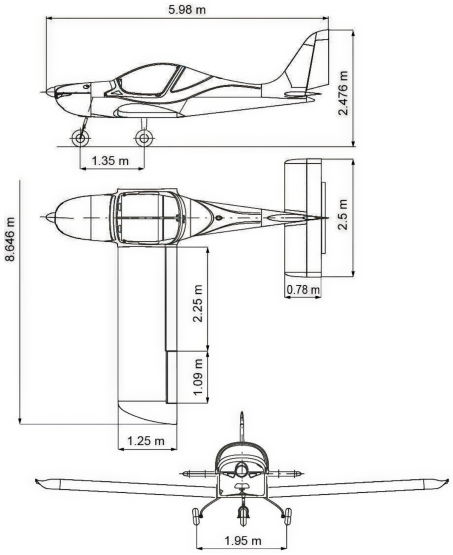

Figure 2.3: Top, front and left side view of the Evektor Sportstar RTC aircraft

The exact geometry of the launch platforms with three firework tubes attached is modelled too and exact measurements of the platforms can be seen in Figure A.1. The fireworks, three per platform, are circular tubes of 30mm diameter and are 600mm long. Two models exist, one with and the other without the launch platforms. For the first case a runway is modelled. Since for CFD models it is common practice to have a non-moving main part, the wing is chosen to be stationary for all cases. This means that the ground should be moving along with the airflow at the same speed. This because a wind-still condition for the CFD models is assumed. The settings for the CFD analysis performed by FloEFD©, an integrated part of Siemens's SolidEdge©, are shown in Appendix A. The settings used are based on the instructions found in reference [43].

Domain	Take-off	Steep turn
x_{min}:	-7.5 m	
x_{max}:	12.5 m	
y_{min}:	0 m (symmetry)	
y_{max}:	10 m	
z_{min}:	-0.601 m	10 m
z_{max}:	10 m	

Table 2.1: Computational domain

The computational domain is taken sufficiently large such that boundary condition at non relevant boundaries are not influencing the results. Table 2.1 gives the size of the used domain. As one can see, to reduce the computational cost, the domain contains a symmetry about the XZ-plane. This means that the minimum dimension in y should be zero as the origin of the domain coincides with the leading edge of the root airfoil section of the modelled wing. Upstream, x_{min}, the domain is less than the downstream domain. With x_{max} being about $^2/_3$ larger in size, it is made sure that the wake of the wing is resolved adequately. With the domain defined, the next logical step is to define the velocities of the objects under investigation in the set domain. These can be seen in Table 2.2 and will be explained further. Depending on the case, there are either two or three (for the take-off case) objects that need a velocity. The first object is straightforwardly the wing model. The reference frame for the simulation is defined such that the wing model is non-moving with all other objects around it having a non-zero velocity. The origin being defined as the leading edge of the root wing section and the x-axis at an angle equal to the angle-of-attack of the wing.

The wing itself is modelled as a stationary real wall with a temperature equal to that of the ambient. The second 'object' is the air filling the remainder of the domain. The initial global mesh is structured with 358 cells in the x-direction, 177 cells in the y-direction and 64, 130 cells in the z-direction for the take-off case and steep turn case respectively. Details about the local meshes for the wing, the runway surface and the refined tip region can be found in Figures A.3, A.4 and A.5. The boundary layer of the wing (and of the runway surface when applicable) is

Object	Velocity (x-only) $^m/_s$	
	Take-off	Steep turn
Air	25.72	30.87
Wing	0	
Ground	25.72	NA

Table 2.2: Object velocities

resolved automatically by the solver using a 2-scale wall function.
The solver employs either the analytic and semi-analytic model with empirical enhancements when appropriate for the flow.[44] Table 2.3 shows the total number of cells, number of cells contacting solid parts and the amount of iterations needed to converge after all refinements. These refinements occur when the values for the chosen goals are converged for the coarser grid. Up to 2 levels of refinement were allowed for these simulations. The resulting meshes for the four cases can be seen in Figures A.6, A.7, A.8 and A.9 found in Appendix A.

CFD simulation meshes				
Case:	1	2	3	4
Total amount of cells:	15269960	14730058	19146691	24873740
Cells contacting solids:	3601486	3577153	3980988	3619434
Iterations:	822	917	533	617

Table 2.3: CFD simulations mesh data

For the take-off case the angle-of-attack between the air and the model is chosen to be 10°. The same goes for the steep turn case as 10°of angle of attack was chosen as well. These angles, when proposed to the team members, were deemed appropriate. A supporting flight test, generating the lift curve for the full aircraft was performed to support the used angle-of-attack for the model. To produce this lift-curve a number of assumptions have to be made. The first one being that the weight of the aircraft is equal to the total lift of the aircraft for level flight. The second one assuming the aircraft weight to be constant while performing the test. Since in real life this is not true, the associated error this introduces has to be estimated. From the POH [41] , the fuel consumption of the aircraft at maximum power setting used during the flight test is known to be $15^{L}/_{h}$. The density of the fuel, an AVGAS type UL91, is approximately $0.72^{kg}/_{L}$. [45] This results, for an estimated time to perform the test of 6 minutes, in a mass loss of $1.08kg$. This is just 0.18% of the maximum take-off mass of the aircraft or 0.21% for the same loaded aircraft but with its fuel tanks of 120L completely empty. These errors are small and they are unlikely to affect the lift curve in such a manner that the curve is no longer usable for the determination of the appropriate angle-of-attack. The actual value of CL, derived for each angle of pitch that was measured, is not of importance as long as the correlation between the CL-values for the flight test is found to be correct. This results in the $\sim CL-\theta$ graph shown in Figure A.22. The difference between the angle-of-attack and the pitch angle is the incidence angle of the wing with respect to the aircraft's longitudinal axis. This angle is graphically obtained from the POH and is found to be approximately 0°. The derived value of CL is obtained by noting the velocity and pitch angle of the aircraft. With these two values known, using the lift equation 2.1 written in a different order, one can calculate the CL value of the entire aircraft. The actual CL_{wing} will be larger in magnitude due to the opposite direction of the lift force generated by the tailplane. $L_{total=L_{mainwing}+L_{htail}}$. Fortunately, only the shape of the lift curve and the stall angle are of importance. The actual values of CL are not used further on this report. It can be observed that at about 10°of pitch, the lift curve tends to start deviating from the quasi linearly increasing part. The 10°is chosen arbitrarily, yet the actual pitch at take-off does seem to be around that pitch angle as observed during the flight test.

$$CL \sim \frac{2 \cdot W}{\rho \cdot V^2 \cdot S} \tag{2.1}$$

Furthermore, the air is moving in the x-direction over the inclined wing model with a velocity of 50kts for the take-ff case; 60kts for the steep turn case. These velocities are converted to SI-units for the simulation. The last object, only valid for the take-off case, is the ground. The ground is modelled as a flat plate, parallel to the x-axis, spanning the entire bottom surface of the domain at a distance of z_{min} from the wing object and moving at the same velocity of the air filling the domain.

2.3. Validating flight tests

To validate the results of the numerical analyses, a number of flight tests were performed. These tests try to mimic the numerical case a far as it was practical, economic and safe to do so. However, no direct comparison should be made between the flight tests and the simulations. This mainly because too many assumptions and simplifications were made on either test. What can be observed from the flight tests is the difference in performance between the aircraft with and without the platforms attached for each test sequence individually. The percent-wise performance changes, either beneficial or disadvantageous, between the simulations and flight tests can be compared to verify if the found changes from the simulations can also be seen in real-life during the flight tests hereby proving or disproving the team leader's claim under investigation.

So first, statistic data such as the one that is acquired during the tests, requires a certain amount of individual test to see a median result provided they are all performed under quasi identical circumstances such as aircraft loading and atmospheric conditions. Possible differences in loading will be normalised by the procedure provided in Section 2.4. Further on this section, possible changes in atmospheric conditions will be discussed. With these elements in mind the same procedure for the test flight was performed five times in an effort to reduce the possible personal bias while keeping the costs of the research flights low. Again, only the percent-wise differences in performance parameters should be compared between flight tests. This allows for the use of two sibling aircraft with minor differences in e.g. trim-tab setting and propeller pitch. This also allows small differences in aircraft balance-wise loading since the loading, other than the fuel and the mass of the two platforms (0.7 kg in total), is not distributed differently during a flight test sequence.

The procedure is performed twice consecutively to maintain the same atmospheric conditions. The procedure is to be executed with the launch platforms attached first. This is solely because of the restriction on the reservation time of the test aircraft. The test flights are all performed at the opening time of the airport, so there is ample time to attach the launch platforms securely. Once the first procedure is completed, the procedure is performed a second time without the launch platforms.

It should be noted that the procedure concerns the take-off case only. This is because more accurate measurement equipment would be required for the steep turn case which would mean a higher cost and possibly time delay if the measurement equipment would not be available at the time of flight testing. Examples of such equipment could be a digital rate of turn indicators with numerical indication instead of the standard visual numberless indicator, a G-load meter typically only found in aerobatic aircraft, a GPS capable of logging the aircraft's position at least every second,... On this non-aerobatic aircraft, used mainly for leisure purposes, this equipment is not present.

The procedure in itself is kept basic, though with as much attention to accuracy as possible. Well before the opening of the airport, the launch platforms are installed and the aircraft fuelled to the exact same amount chosen for all the flights. The fuel amount is verified both visually with a mark and digitally by the fuel measure with an inaccuracy of one litre. On a total capacity of 120 litres, this should yield an inaccuracy of more than 1% which seems plausible given the safety standards used for aviation. Knowing the amount of fuel together with the exact weight of the aircraft as stated in the official weighing report and the weight of the two crew members for the test flight, the total weight at take-off can be noted.

Consistent take-off configuration is assured by using a 'stick-free' elevator trim setting of the aircraft before lift-off. This means that the elevator trim of the aircraft is set to exactly the same mark for all the test flights to be performed. This mark can, again, be seen digitally. 'Stick-free' means in this case that, during the ground roll acceleration phase of the take-off, the stick is allowed to move freely sliding back and forth between the arms of the pilot, merely to allow for immediate roll input if such would be required upon rotation of the aircraft. This way the aircraft will rotate by itself without input of the pilot, eliminating another possible error source. Prior to the test flights, a suitable elevator trim setting is to be determined. This setting should be such that the aircraft doesn't rotate before reaching at least it's stall speed for that configuration and weight thus preventing take-off stall. The setting should also allow for the aircraft to rotate before reaching the end of the available runway. A suitable setting is found at $^3/_4$ of fully aft elevator trim.

The lift-off of the aircraft is quite abrupt so it clearly defines the moment when to note the lift-off airspeed. The airspeed is shown with an accuracy of 0.5 knots. E.g. if an airspeed of 50 knots is shown to the copilot, the actual value may be in the range of 49.5 to 50.4 knots. Since the pilot has to immediately push the stick forward and consequently re-trim the aircraft for climbing flight, the

airspeed at lift-off has to be recorded by the copilot. Several of these 'copilots' are used to mitigate his or her personal bias on the exact moment of lift-off and its consequent airspeed. Only the results of a single test sequence are to be compared and the personal bias is not assumed to change during a sequence. Therefore the effect of the copilot's bias is assumed to not affect the overall outcome of a testing sequence.

Another possibility would have been to measure the take-off distance. This could be done by placing one or more camera's along the runway outside the obstacle free zone's surrounding the runway. These camera's should be placed such that they record the expected location where the aircraft might take-off. Marker lines would have to be drawn across the 45 meter wide runway to be able to measure the take-off distance accurately. Minor wind gusts < 5 knots would have a large impact on the distance. They can indirectly be read-off from the airspeed indicator as an increase in airspeed. The aircraft will therefore lift off earlier since it has already achieved the required airspeed for lift-off under the same circumstances (trim setting, weight, loading, atmospheric conditions, ...) With this in mind, this option was not pursued further and the previously mentioned recording of the airspeed at lift-off is chosen.

So, after take-off, the pilot continues to fly a standard circuit pattern followed by a full stop landing. He vacates the runway and taxi-es the aircraft back to the position where he noted the take-off fuel and executes the same procedure for two more times. This provides three data points with fuel volume and lift-off speed.

Upon completion of the three take-off's with the launch platforms attached. They are removed on the apron and carried on board the aircraft to still account for their, though very small, weight. The sequence is repeated in the same fashion as the first, but now without the firework launch platforms attached.

Provided that the testing sequences can occur consecutive, the atmospheric parameters such as density, pressure and humidity, are assumed to not have changed in the estimated required time of an hour and a half for the sequences to be completed. This is to ensure that the air density during the test sequence can be assumed to be constant. [46] Therefore the air pressure at sea level, called 'QNH' in aviation, is recorded for each sequence along with the ambient air temperature. With these two parameters known, the density can be derived through the ideal gas law applied to air as provided in equation 2.2.

$$\rho = \frac{P}{R_{air} \cdot T} \tag{2.2}$$

The pressure P and temperature T are taken from the METAR's of surrounding airports to check the immutability during the test sequence. The immutability of the air gas constant is checked by the dew point temperature given in the same METAR's. *The dew point of a given body of air is the temperature to which it must be cooled to become saturated with water vapor.*[47] The air pressures and temperatures as stated in the METAR's of the surrounding airfields EBOS (Ostend, Belgium), EBBR (Brussels, Belgium) and LFQQ (Lille, France) are given in Table A.1 found in appendix A. The full METAR text's are available online[48]. The influence of a change of $1hPa$ pressure e.g. 1014hPa instead of 1013hPa, changes the density by 0.001%. The influence of a change of 1 degree temperature e.g. 16°C instead 15°C changes the density by 0.003%. (note the conversion to Kelvin!) it is therefore concluded that the assumption made regarding the constant density is valid for this experiment.

2.4. Results processing & normalisation

Upon completion of the flight tests a number of raw flight test data is expected to have been obtained. All results should be of the same format as to be used in Table 3.2 though the medium to record the data was left up to the copilot's discretion. Per flight test there will be a total of six data entries each consisting of the fuel volumes in the aircraft's tanks and the airspeed at which the aircraft loses contact with the ground. These data entries will then be grouped and written down in a table for easy examination.

The raw data is consequently further processed by normalising both test cases, with and without the firework launch platforms attached, for each flight test. Since no aircraft balance data is know, it can not be safely assumed that the lift coefficient at lift-off is exactly the same for each flight test. No load shifting was intentionally done and the launch platforms, once detached, were placed inside the aircraft at about the same longitudinal position to maintain the same loading. Given the same aircraft

balance, equation 2.5 can be used to normalise the VLOF's of the clean case with those with the platforms attached. The data is also normalised to the same meteorological conditions at the time of the first test flight using equation 2.2 and Table A.1. The basic formula used is the well-known Bernoulli equation which is valid for incompressible flows. To calculate the error margin on the resulting lift-off speeds, the possible error on pressure, temperature, mass and read-off take-off speed is assumed to be ±0.5 the value of the physical quantity for each quantity. The norm is the factor by which the airspeed of the clean test case needs to be multiplied with to account for the weight loss due to the fuel consumption and the offset of the meteorological conditions from the ISA standard at mean sea level. A high norm and low norm are also calculated. Hereby, the highest possible and lowest possible values of the take-off speed are defined resulting in an error margin on the provided data. 2.6

$$\frac{W^*}{W} = \frac{0.5 \cdot \rho \cdot S \cdot C_l \cdot {VLOF^*}^2}{0.5 \cdot \rho \cdot S \cdot C_l \cdot VLOF^2} \Longrightarrow normalise\ W \tag{2.3}$$

$$\frac{\rho^*}{\rho} = \frac{\frac{P^*}{R_{air} \cdot T^*}}{\frac{P}{R_{air} \cdot T}} = \frac{P^* \cdot T}{P \cdot T^*} \Longrightarrow normalise\ \rho \quad (P = 1013\ hPa,\ T = 288.15\ K) \tag{2.4}$$

$$F = \sqrt{\frac{W^* \cdot \rho}{W \cdot \rho^*}} \tag{2.5}$$

$$VLOF^* = F \cdot VLOF \tag{2.6}$$

3

Test case results

This chapter features the results of the CFD simulations performed on the models created for the two cases as well as the results of the validating real life flight tests by the team's wingman and his copilots. The first section (3.1) contains the results of the take-off case and the steep turn case for both the model with and the model without the firework launch platforms. The second section (3.2) gives the results obtained from the real life flight tests. Larger figures than the ones shown in this chapter are available in Appendix A.

3.1. CFD simulation case results

The two CFD simulation cases, as described in Section 2.1, are the take-off and the steep turn case. Both feature a high angle-of-attack inducing spanwise flow with more pronounced wingtip vortices as know from Chapter 1. First the take-off case results are provided and discussed in Subsection 3.1.1. The clean wing and the wing with the firework launch platforms attached are set side-by-side graphically to visualise the effect of the launch platform on the flow. For the steep turn case, the same is done in subsection 3.1.2. The Table 3.1 contains the numerical data of both the test cases with a separate value for the launch platform by itself. It should be noted that the data for the cases is provided for the entire model, so also the forces generated by the mirrored part are added. This is why the values for the outwards, quasi spanwise forces along the Y-axis, are equal to zero. The force in Y generated by the mirror parts is equal and opposite in direction thus nullifying the total resultant force in Y. For the launch platforms only one of both platforms is considered.

Case nr.:	Airspeed:		Resultant force	X-axis, drag	Y-axis outwards,	Z-axis, lift
1:	50 knots	F (N)	4621.9	184.5	0.0	4618.3
Take-off	25.72 m/s	μ (N)	33.3	33.3	0.0	-0.1
2:	50 knots	F (N)	4624.4	185.8	0.0	4620.6
Take-off	25.72 m/s	μ (N)	33.5	33.5	0.0	-0.1
		F_p (N)	2.1	0.9	1.7	-0.9
		μ_p (N)	0.2	0.2	0.0 (+)	0.0 (-)
3:	60 knots	F (N)	5762.6	404.0	0.0	5746.8
Steep turn	30.87 m/s	μ (N)	54.0	54.0	0.0	-1.0
4:	60 knots	F (N)	5786.9	380.7	0.0	5774.4
Steep turn	30.87 m/s	μ (N)	54.1	54.1	0.0	-2.1
		F_p (N)	2.4	1.6	1.6	-0.8
		μ_p (N)	0.3	0.3	0.0 (+)	0.0 (-)

Table 3.1: CFD simulation data

3.1.1. Take-off case results

Case 1 & 2, as found in Table 3.1, provide the results of the computational flow simulations performed on the model for the take-off case. Note the simplifications made to the model as stated in 2.2. From the simulation data of the two first cases, one can derive the following relevant parameters. Compared to the first case, the second case, the one with the launch platforms attached, features a lift force increase of 0.05%. Meanwhile, the drag force is increased by 0.7% even though the launch platforms by itself already deliver 2 * 0.9 N of drag force. The total drag increase of just 1.3 N instead of an expected 1.8 N suggests a possible decrease in another drag source. An extra object on the wing is expected to add some drag to the aircraft which is translated to the increase in total friction drag F_p of 0.6%. Even though the total drag is increased resulting eventually in a decrease of lift-to-drag ratio of 0.4%, a decrease in one of the drag components is presumed. The convergence history of the cases is shown in Figures A.18, A.19, A.20 and A.21 to be found in Appendix A.

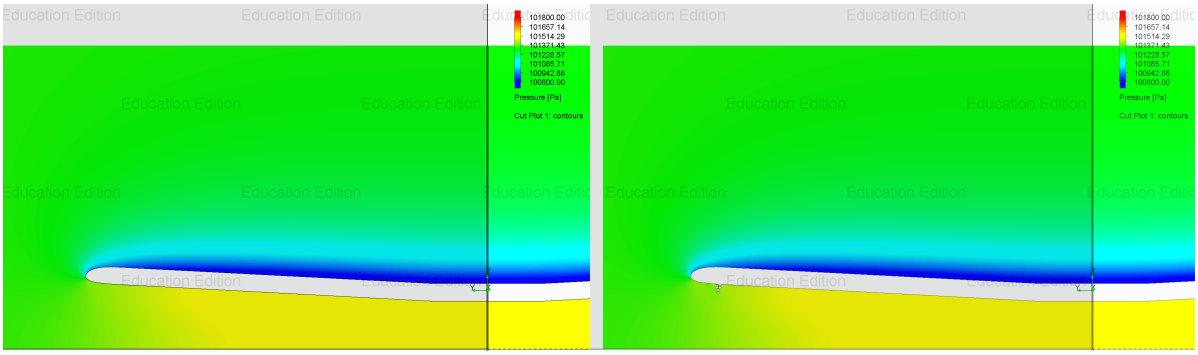

Figure 3.1: Left: clean wing, Right: wing with launch platform

Figure 3.1 shows a spanwise cross-section of the aircraft at 0.25 times chord measured from the leading edge. The figure itself is a composition of two separate images. The part on the right is taken from the clean wing model. The part on the left is taken from the wing model with the launch platforms attached simulation results. At first glance, the left and right image appear very similar to each other. If one were to look closer on the launch platform, as can be seen in Figure 3.2, one can see a higher pressure area on the inboard side of the launch platform and a lower pressure area on the outboard side. The pressure contours also show a more vertical profile under the launch platform as compared to the clean wing case. Therefore, a certain amount of blocking of the spanwise flow could be assumed from the overall pressure contours under the wing. The assumption of the blocking is confirmed if one were to look at the streamlines under the wing as can be seen in Figure 3.3. The streamlines for the first case, the clean wing, visually bend slightly more towards the wingtip as the flow proceeds to roll up once it leaves the trailing edge of the wing. Figure 3.3a displays the streamlines on the underside of the wingtip. For the second case, by looking at Figure 3.3b, one can see a clear disturbance of the flow by the launch platforms. A clear blocking of the flow can be observed going from the leading edge towards the aft part of the launch platform and even further aft up to about 70% of the wingspan. The blocking of the flow can also be observed from the side force on the platform as suggested in Section 1.4. This side force is about 1.7 N of force in magnitude and almost twice the drag force of the platform. At the outboard side of the platform the streamlines bend inboard again due to the lower pressure region just outboard of the launch platform deflecting the flow from going to the wingtip. The streamlines of the turbulent region, originating at the forward contact point of the

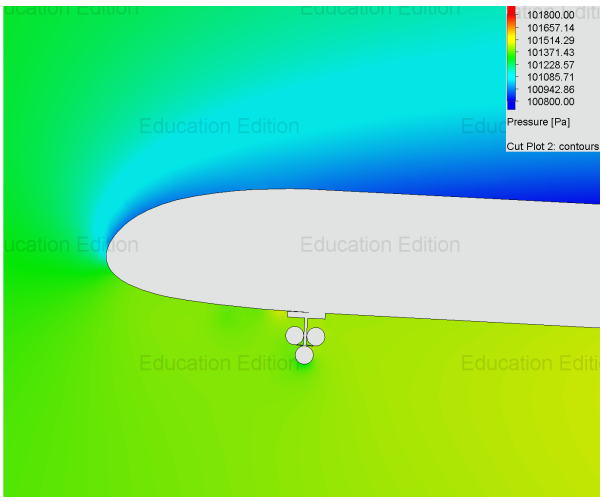

Figure 3.2: Case 2: detail view

launch platform with the wing, can be seen in Figure 3.3b too.

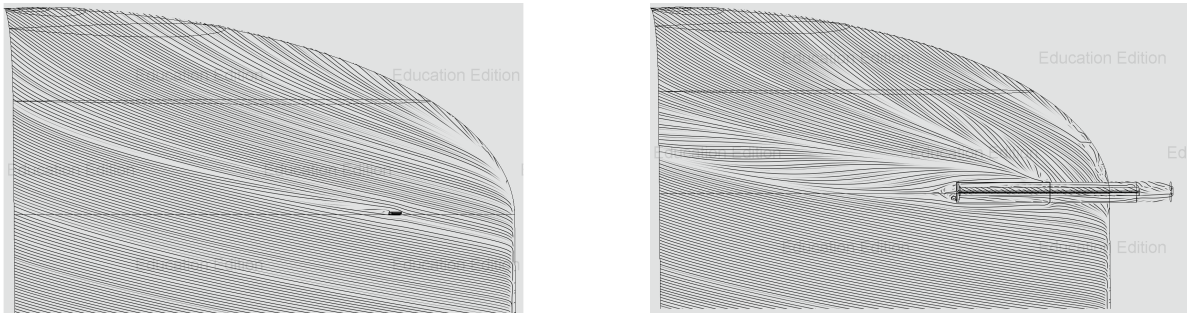

(a) Case 1: Clean wing with attachment eye visible

(b) Case 2: Launch platform attached

Figure 3.3: Under-wing streamlines near the wingtip

3.1.2. Steep turn case results

The results for the steep turn cases can be found in Table 3.1 under case 3 & 4. From the table, the relevant parameters for the steep turn case are found to be the following. The lift is increased by 0.5% which is considerably more than the increase found for the take-off case.

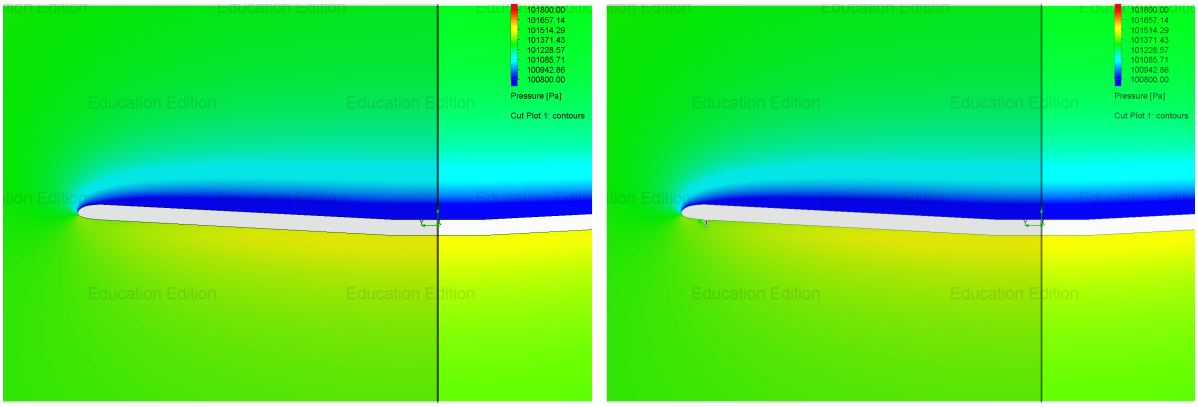

Figure 3.4: Left: clean wing, Right: wing with launch platform

Even more important is the decrease in drag of 5%. The friction force is increased by 2.4%. With the results of lift and drag already known, It seems obvious that the lift-to-drag ratio is increased. This has been increased by 7%. From Figure 3.4 one may observe that there is only very little evidence, if any, of blocking of the spanwise flow. Looking closer at the launch platform, one sees that there is also a low pressure area outboard of the launch platform, but in this case more pronounced when compared to the take-off case. The pressure contours for the steep turn case are similar to one another as was the case for the take-off cases. A possible explanation for this is likely the very small differences the launch platforms generate. The reduction of the lift induced drag as could be assumed for the take-off case has now even become more likely. The spanwise flow is effectively blocked by the platform to a certain degree. Looking at the streamlines as can be seen in Figure 3.6, one can see see the presence of the flow blocking. The streamlines of the platform attached case as seen in Figure 3.6b are bent back to the inboard side when compared to those of the clean wing case seen in Figure 3.6a. The tendency to bend inboard again as found to a lesser amount for the take-off case is now more pronounced. Another thing one can observe is the wake behind the platform.

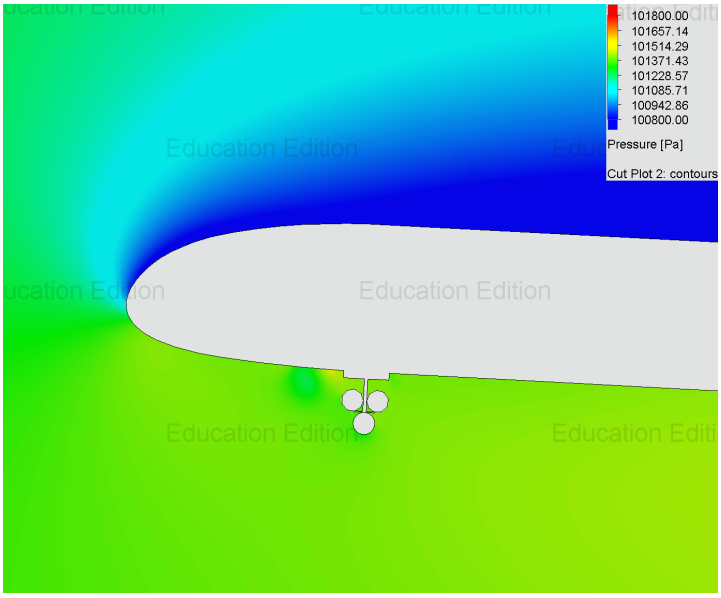

Figure 3.5: Case 4: detail view

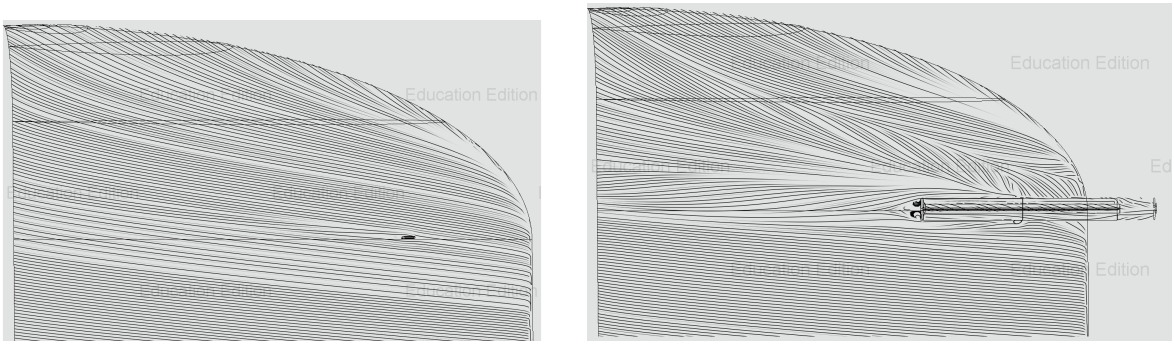

(a) Case 3: Clean wing with attachment eye visible

(b) Case 4: Launch platforms attached

Figure 3.6: Under-wing streamlines near the wingtip

3.2. Flight test results

This section provides the data and observations of the results obtained from the real life flight testing of the firework launch platforms. The obtained date can be found in Table 3.2. The meteorologic parameters, confirming the immutability of the air density during a test sequence, can be found in Table A.1 in Appendix A.

The first observation that can be made from Table 3.2 is that the first three flight tests were performed at the same take-off mass (TOM) ($\Delta < 0.36\%$). A second observation that can be made is that the influence of the difference in TOM ($\Delta = 3.09\%$) is not directly reflected in the lift off speed. The fuel tank, from which the aircraft's engine is fed was not changed during a circuit series of a flight test. This can be seen from either the left of right fuel tank remaining at the same fuel volume from the beginning of a circuit series of a flight test. It is noted that the fuel consumed by the OO-VMA was about 10 litres (7.2 kg) for a flight test. For the OO-VMD this was 4 litres (2.9 kg). The first equates to less than 1.31% of the take-off mass of the OO-VMA. The latter to less than 0.53% of the take-off mass of the OO-VMD. Both are maximum difference percentages. The lowest take-off mass of all flight tests per aircraft is used as a reference for the percentages. Table 3.3 shows the same table but with the clean lift-off speeds normalised by weight to those of the ones with the platforms attached using the normalisation coefficient F as defined in Equation 2.5.

From Table 3.3 it can be seen that, given the resolution of the recorded data, the differences with the raw data are minimal. The changes are very small. The coefficient F is shown with more significant digits to see the actual used value to obtain the lift-off speeds. The lowest and highest possible value

Aircraft:	TOM:	Flight test nr.:	Circuit nr.:	Platforms attached			Clean		
				L tank	R tank	VLOF	L tank	R tank	VLOF
OO-VMA	550kg	1	1	45	44	52	41	44	53
			2	42	44	53	39	44	54
			3	41	44	52	35	44	54
OO-VMA	550kg	2	1	48	45	54	46	40	55
			2	48	42	53	45	40	54
			3	48	40	54	43	40	54
OO-VMD	552kg	3	1	39	37	55	37	37	55
			2	38	37	56	36	37	54
			3	37	37	54	35	37	54
OO-VMA	567kg	4	1	45	45	53	40	45	55
			2	44	45	53	40	41	56
			3	40	45	54	40	40	55
OO-VMD	565kg	5	1	37	43	53	36	40	56
			2	37	42	52	36	39	57
			3	37	41	52	36	38	56

Table 3.2: Raw flight test data. Fuel in litres, speed in kts.

of the coefficient and lift-off speed are calculated too to shown the error margin on the value. These normalised lift-off speeds are consequently averaged per flight test. For a flight test, the values of the three circuits with the platforms attached are averaged. The same is done for the values without the platforms. The results can be seen in Table 3.4. This table includes averaged velocities per flight test with and without the launch platforms attached along with their respective margins, the percent difference in lift-off speed for when the platforms are attached and the overall average of the speed reduction for the five flight tests. The overall error margin is taken as the largest and smallest error calculated from all of the flight tests. This results in a reduction of lift-off speed of 2.2% with the launch platforms attached as compared to the clean wing. The error margin, however, is fairly large ranging from a maximum reduction of 6.8% to an increase of 1.5%. It is observed that the first four flight tests provide a sensible outcome with the fifth flight test appearing to be the odd one out. A larger number of flight tests would results in the possibility to rule out outlying results.

Aircraft:	TOM:	Test nr.:	Circuit nr.:	Platforms attached							Clean wing						
				TOM	F -	coeff. F	F +	V -	$VLOF^*$	V +	TOM	F -	coeff. F	F +	V -	$VLOF^*$	V +
OO-VMA	550kg	1	1	550	1.0172	1.0188	1.0205	52	53	54	545	1.0126	1.0142	1.0158	53	54	54
			2	547	1.0144	1.0160	1.0177	53	54	54	543	1.0107	1.0123	1.0139	54	55	55
			3	545	1.0135	1.0151	1.0167	52	53	53	539	1.0070	1.0086	1.0102	54	54	55
OO-VMA	550kg	2	1	550	1.0331	1.0348	1.0365	55	56	56	543	1.0265	1.0282	1.0298	56	57	57
			2	547	1.0303	1.0320	1.0336	54	55	55	542	1.0256	1.0272	1.0289	55	55	56
			3	545	1.0284	1.301	1.0317	55	56	56	540	1.0237	1.0253	1.0270	55	55	56
OO-VMD	552kg	3	1	552	1.0240	1.0257	1.0273	56	56	57	550	1.0222	1.0238	1.0255	56	56	57
			2	551	1.0231	1.0247	1.0264	57	57	58	549	1.0212	1.0229	1.0245	55	55	56
			3	550	1.0222	1.0238	1.0255	55	55	56	547	1.0194	1.0210	1.0227	55	55	56
OO-VMA	567kg	4	1	567	1.0138	1.0154	1.0170	53	54	54	562	1.0094	1.0109	1.0125	55	56	56
			2	566	1.0129	1.0145	1.0161	53	54	54	558	1.0058	1.0073	1.0089	56	56	57
			3	562	1.0094	1.0109	1.0125	54	55	55	557	1.0049	1.0064	1.0080	55	55	56
OO-VMD	565kg	5	1	565	1.0209	1.0225	1.0241	54	54	55	561	1.0173	1.0189	1.0205	56	57	58
			2	564	1.0200	1.0216	1.0232	53	53	54	560	1.0163	1.0179	1.0195	57	58	59
			3	563	1.0191	1.0207	1.0223	52	53	54	559	1.0154	1.0170	1.0186	56	57	58

Table 3.3: Normalised flight test data. Fuel in litres, speed in kts. For F see 2.6

Aircraft:	TOM:	Test nr.:	Platforms attached			Clean wing					
			Avg -	Average	Avg +	Avg -	Average	Avg +	Δ -	Δ	Δ +
OO-VMA	550kg	1	53	53	54	54	54	55	-2.0%	-2.0%	-2.0%
OO-VMA	550kg	2	55	55	56	55	56	56	-0.7%	-0.7%	-0.7%
OO-VMD	552kg	3	56	56	57	55	56	56	1.4%	1.4%	1.5%
OO-VMA	567kg	4	53	54	55	55	56	56	-3.1%	-3.1%	-3.1%
OO-VMD	565kg	5	53	53	54	57	57	58	-6.8%	-6.7%	-6.7%
								Overall speed reduction with error margin:	-6.8%	-2.2%	1.5%

Table 3.4: Normalised and averaged flight test data with error margin.

4

Conclusion & Recommendations

This report investigated the claim made by the lead of formation Team The Whiskeys. He claimed that by attaching the fireworks launch platforms, made on the occasion of the re-opening of their local flying club, the aircraft used by the team became more performing i.e. able to make sharper turns, lift-off earlier, etc. The claim resulted in the research question whether or not the aircraft lifts off at a lower airspeed with the launch platforms attached and if there's more lift available for the same angle-of-attack to make a steeper turn. This claim is found to be possible but unlikely noticeable as shown by this report. The results obtained from the CFD simulations performed on models of the aircraft, made specifically for the simulations, show that indeed an increase in lift force and lift-to drag ratio are present for the steep turn situation. This while the drag force is reduced even with the platforms being an extra source of drag. Clear blocking of the spanwise flow component due to the launch platforms has been established and is visual, but also measurable as an outwards pointing side force on the launch platforms. This results for the steep turn case in an increase in lift of 0.5%, a decrease of the aircraft's drag of 5.0% and consequently an increase in lift-to-drag ratio of 7.0%. For the take-off case however, the simulation shows an increase in lift of 0.05%, a drag increase of 0.7% and thus an decrease in lift-to-drag ratio of 0.4%.

The reason why this is not a full confirmation of the claim regarding the steep turn or a rejection of the statement for the take-off case is mainly the possible modelling error for the CFD simulations. This because no interference effects are investigated due to the simplicity of the model. A 3D scan of the aircraft, nowadays possible, could eliminate this error largely. On the other hand, the real life tests can't confirm the CFD results since the results of the tests all fall well within the possible error margin of the experimental setup used. Even though the raw data may suggest a potential increase in performance by an average lift-off speed reduction of 2.2%, it can not be shown with any certainty because of the error margin of -6.8 to 1.5% speed increase. Moreover, the felt 'performance increase' as claimed by the team's leader is way more than the amount of increase the CFD simulations suggest.

This does not mean that more real life tests would not be chase-worthy. To pursue an accurate result of the real life behaviour of the fireworks launch platforms, test equipment with a finer resolution needs to be used along with a larger sample size of at least 30 flight tests or more [49] to reduce the error margin. Also, more objective measurement of the lift-off moment in time should be made. Lidar or laser distance measurement between the aircraft's hull and the ground are amongst the possible solutions to resolve this uncertainty. Finer resolution and more accurate measurement are expected to come at a higher cost. A redesigned version of the platforms having a more aerodynamic shape based on the results gathered in this report, may therefore be worthy of a second investigation with more accurate measurement equipment. It can also be noted that downward facing wingtip devices should be investigated further since only a limited amount of research is available to date. An analysis of the effect of angle-of-attack on the performance of the launch platforms might also be interesting provided one assumes the same effects happening as with the vortilons in section 1.3.

A

Figures

Airport :		EBOS		EBBR		LFQQ		EBUL	
Day	Time	QNH	T	QNH	T	QNH	T	QNH	T
20/01/2023	14:30 - 15:30	1016	6	1014	5	1016	5	1015	5
21/01/2023	10:00 - 11:00	1033	3	1032	0	1032	1	1032	1
29/01/2023	13:00 - 14:00	1025	5	1025	3	1026	4	1025	4
03/02/2023	13:00 - 14:00	1031	9	1029	11	10331	12	1030	11
04/02/2023	10:00 - 11:00	1037	8	1037	9	1037	10	1037	9

Table A.1: METAR data for surrounding airports with unofficial data for EBUL

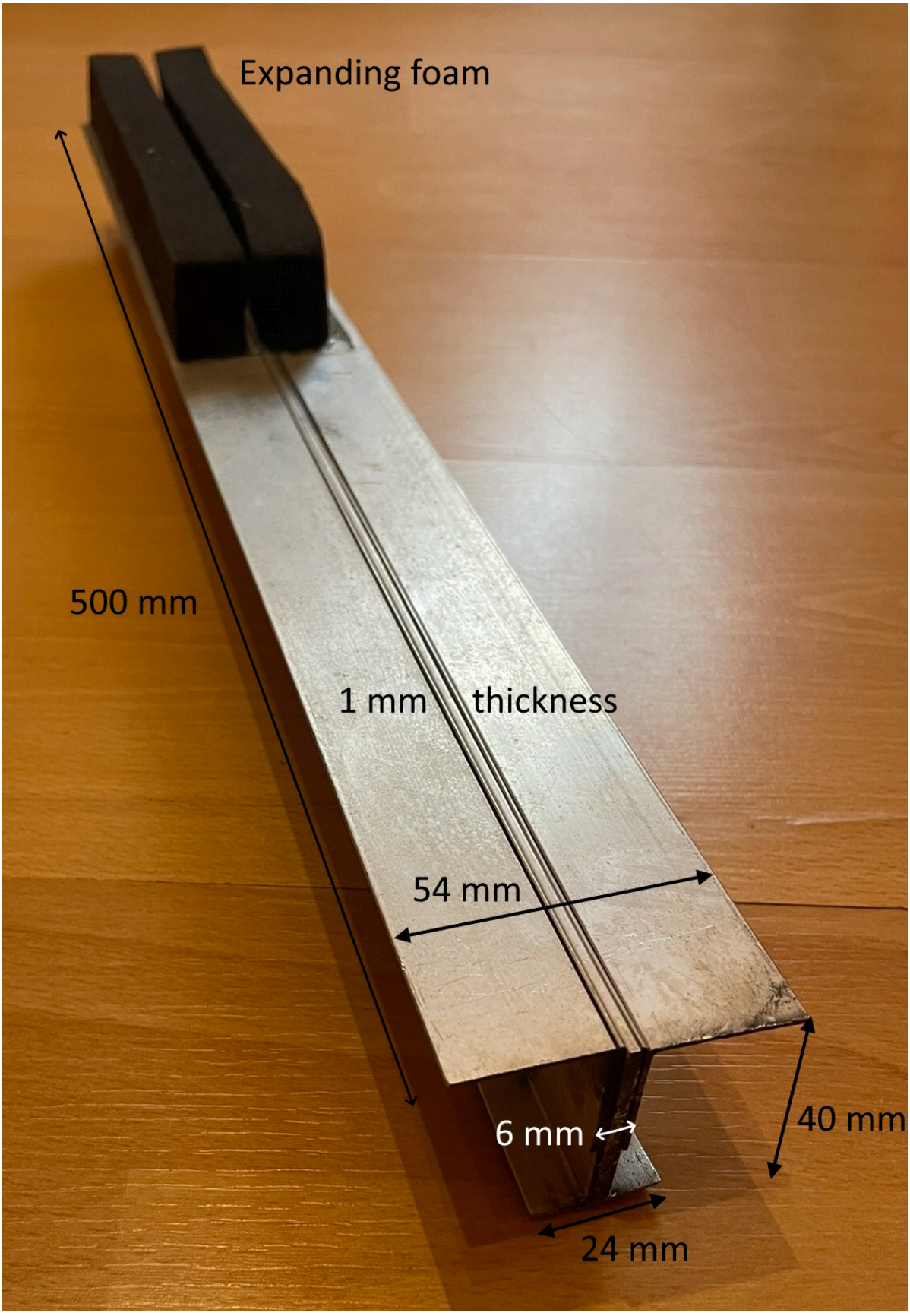

Figure A.1: Dimensions of a fireworks launch platform, mass = 0.35 kg

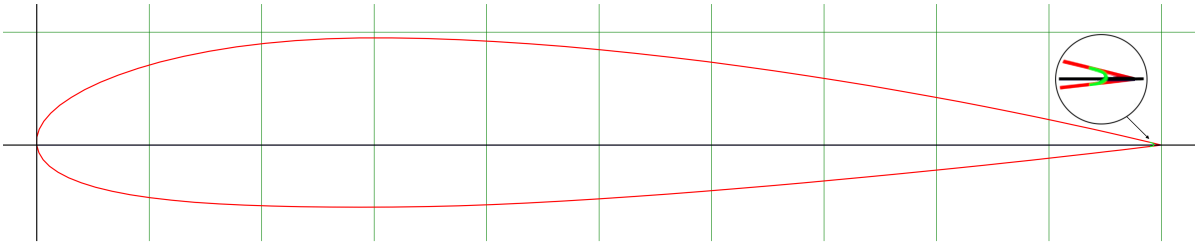

Figure A.2: NACA 2315 mod with indication of the modified trailing edge

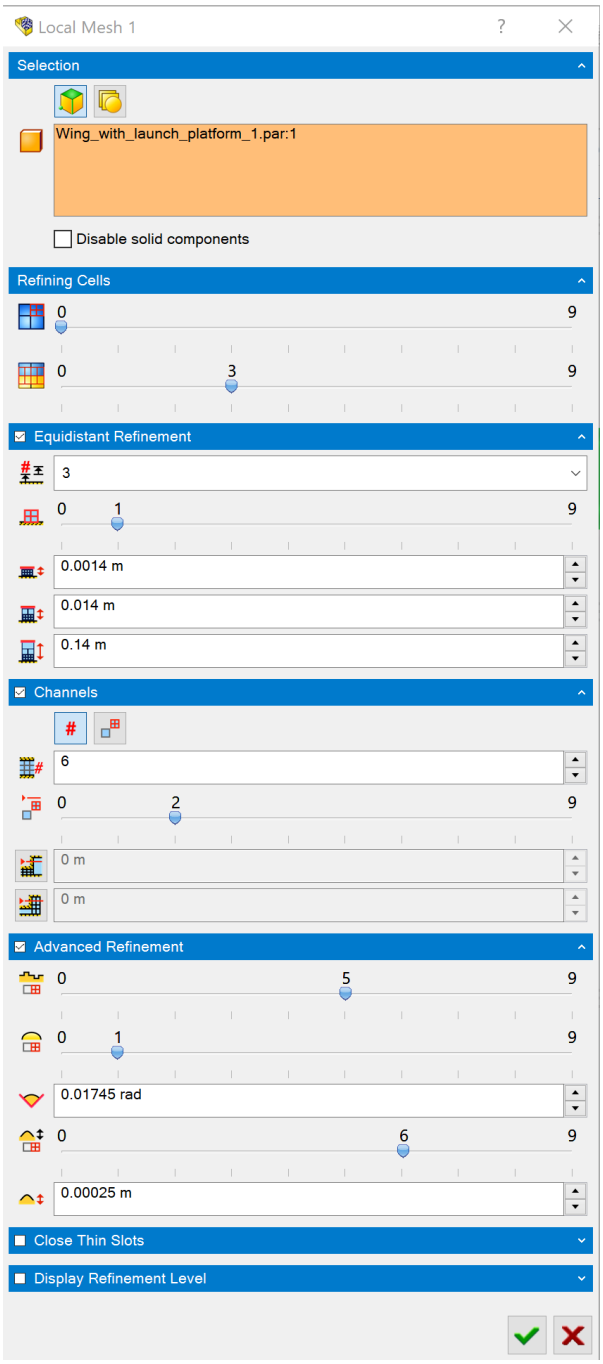

Figure A.3: Local mesh settings for the aircraft's wing.

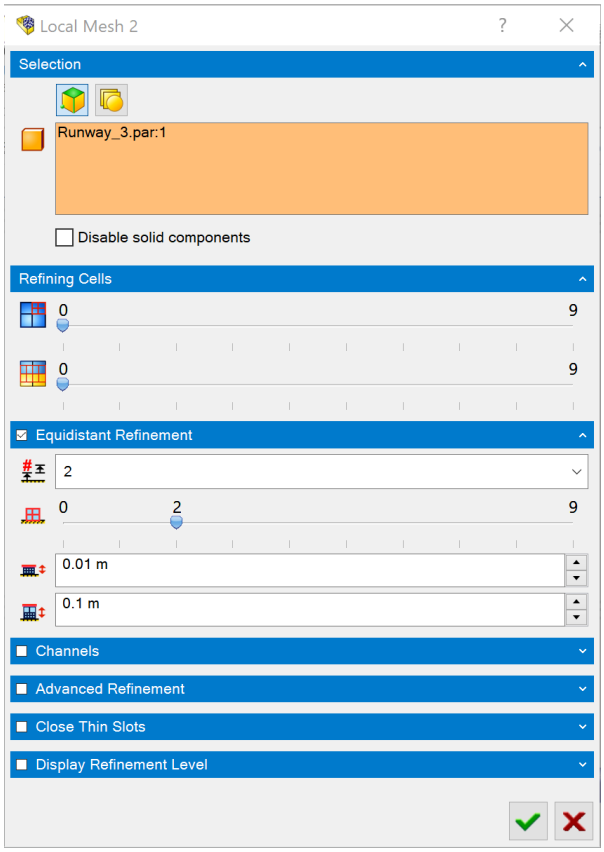

Figure A.4: Local mesh settings for the runway surface.

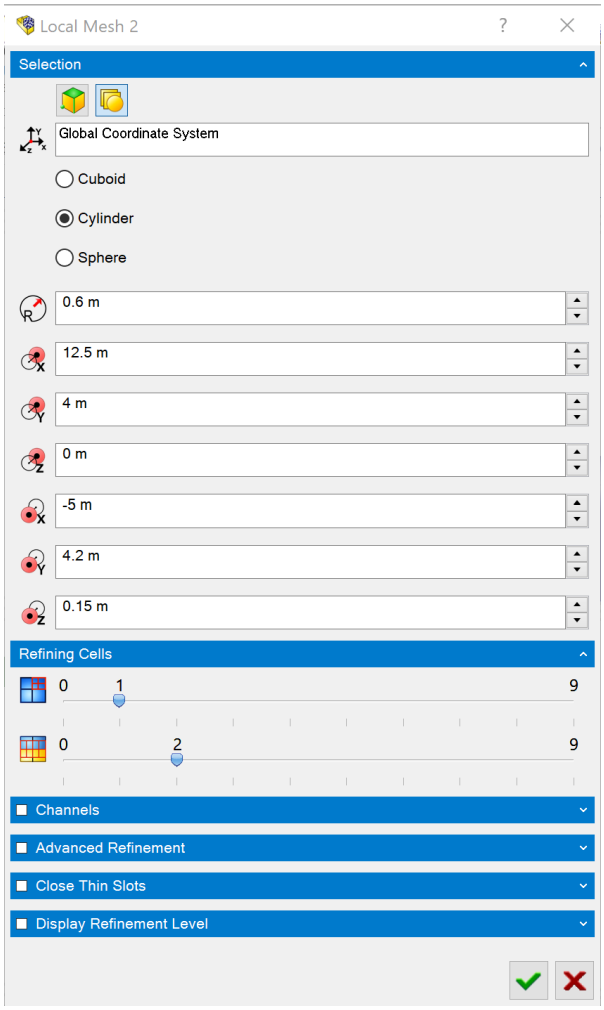

Figure A.5: Local mesh settings for the wing's tip region.

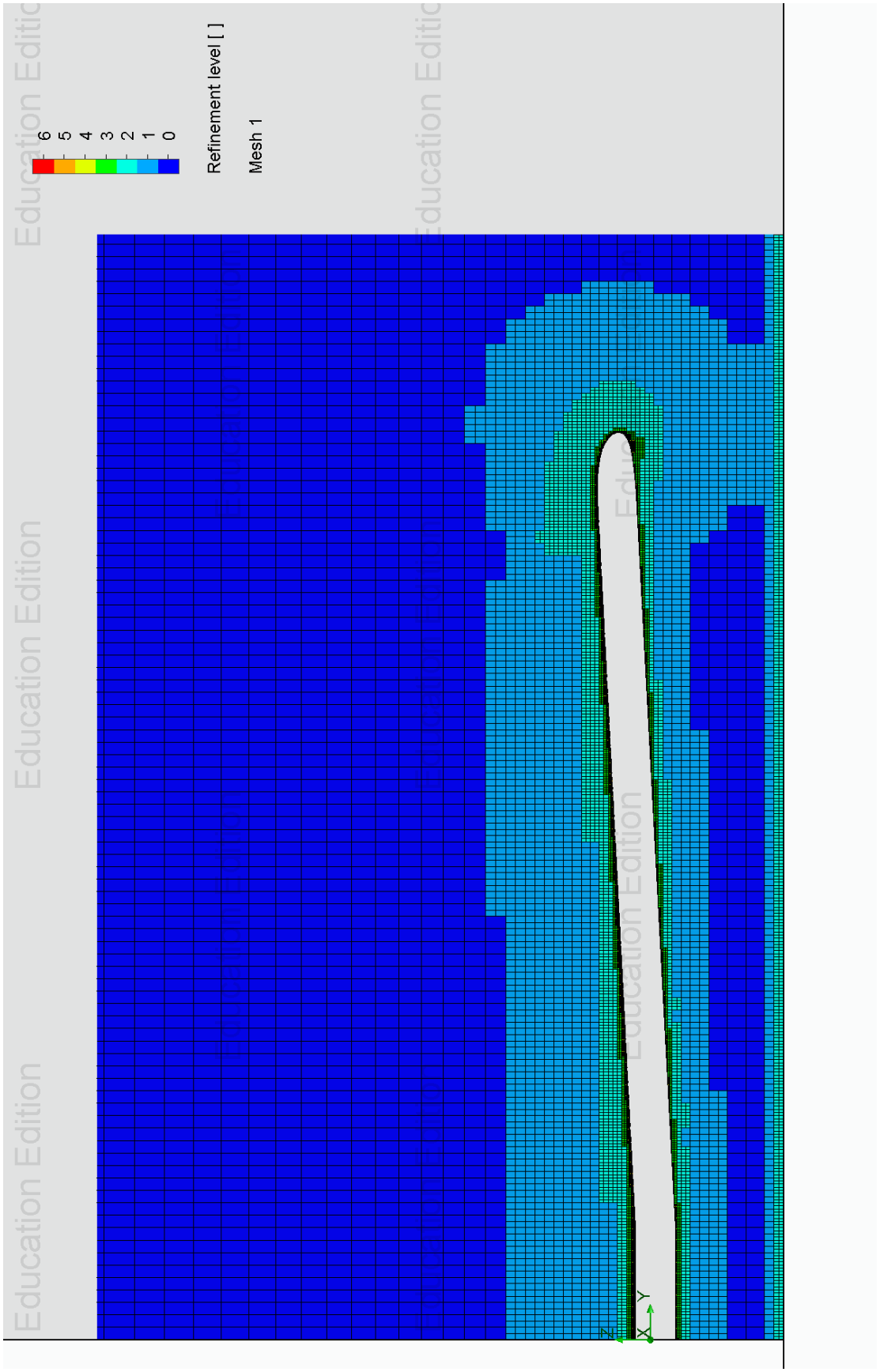

Figure A.6: Mesh for the clean wing for case 1.

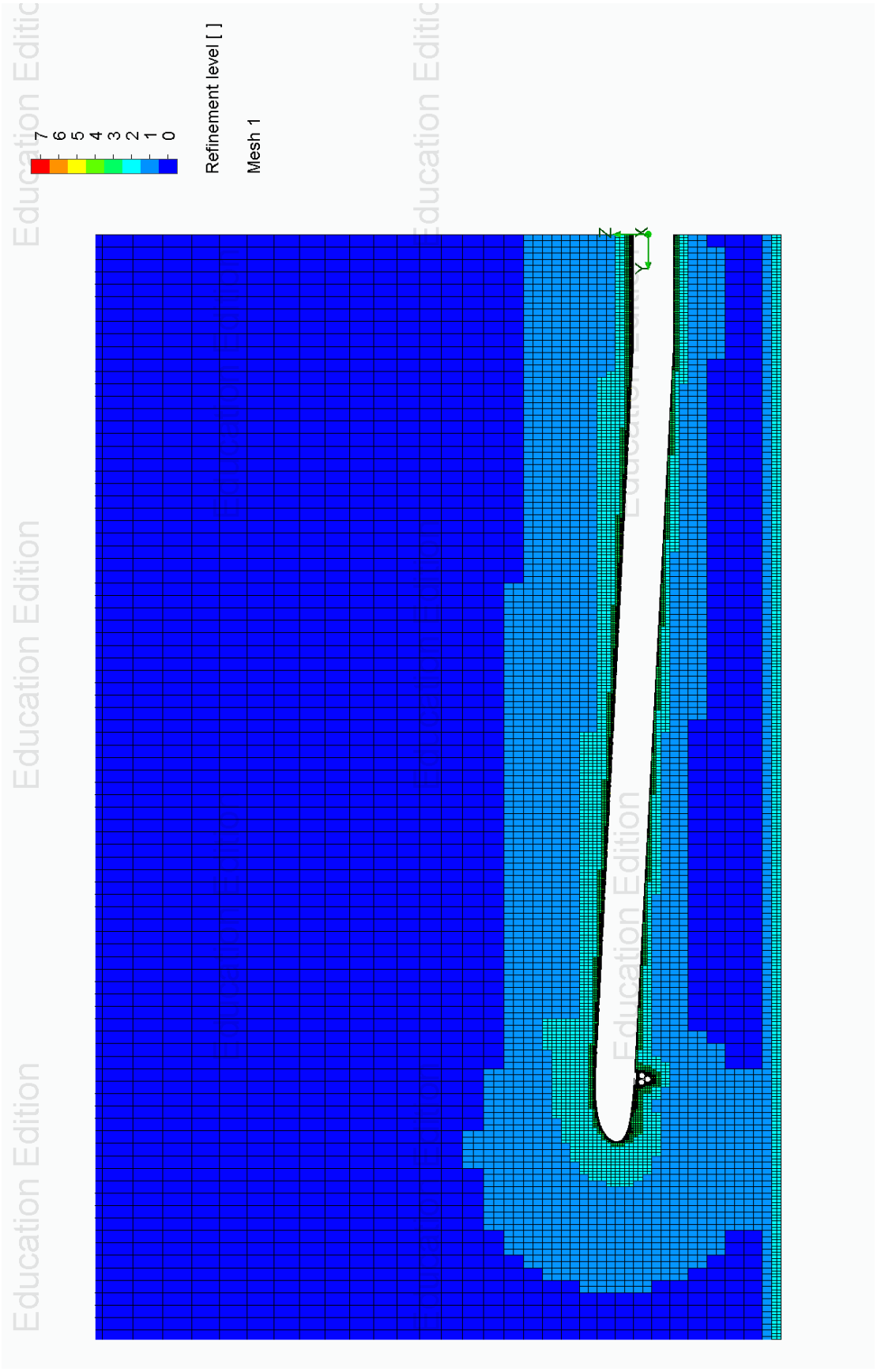

Figure A.7: Mesh for the wing with attachments for case 2.

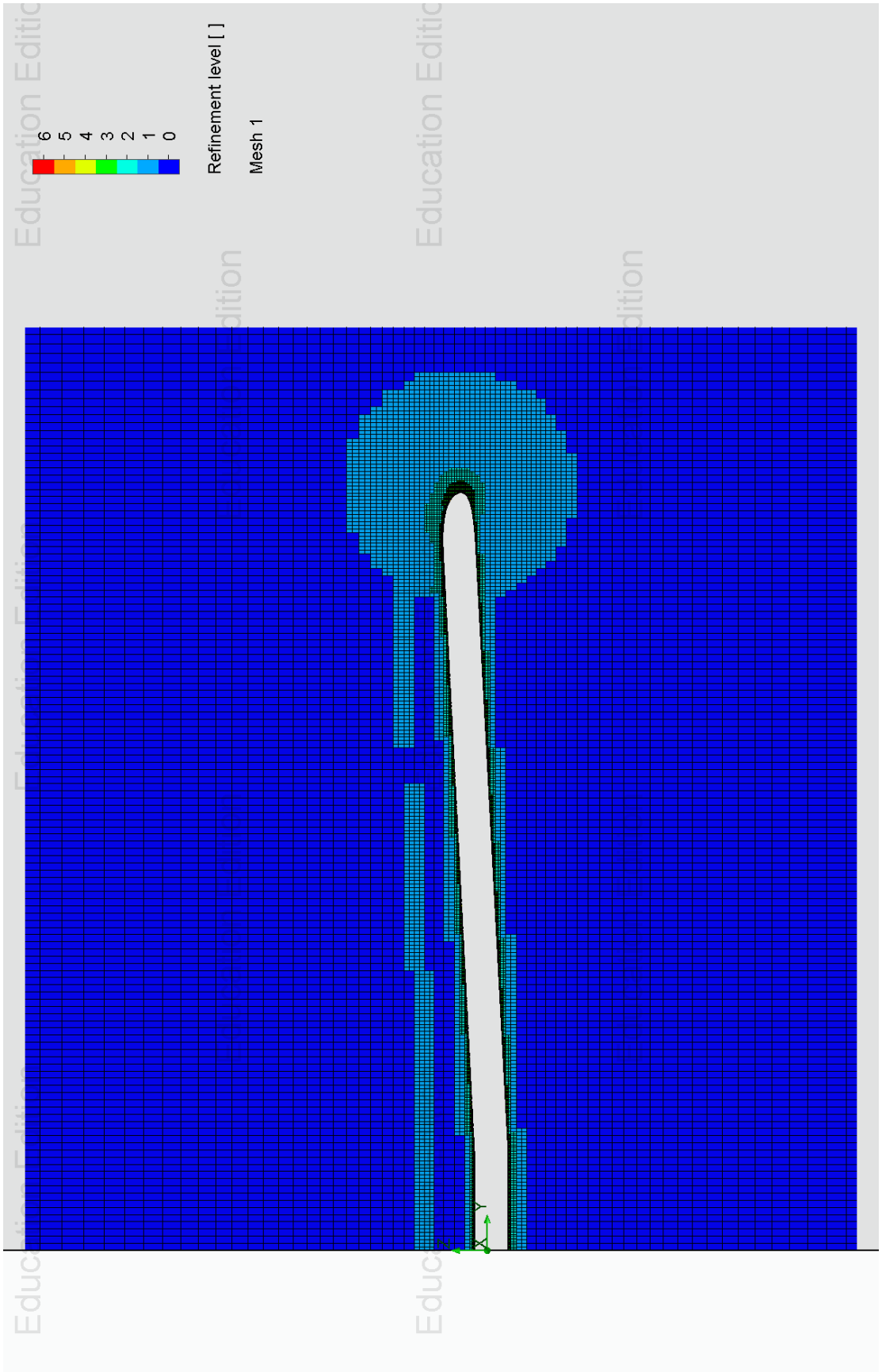

Figure A.8: Mesh for the clean wing for case 3.

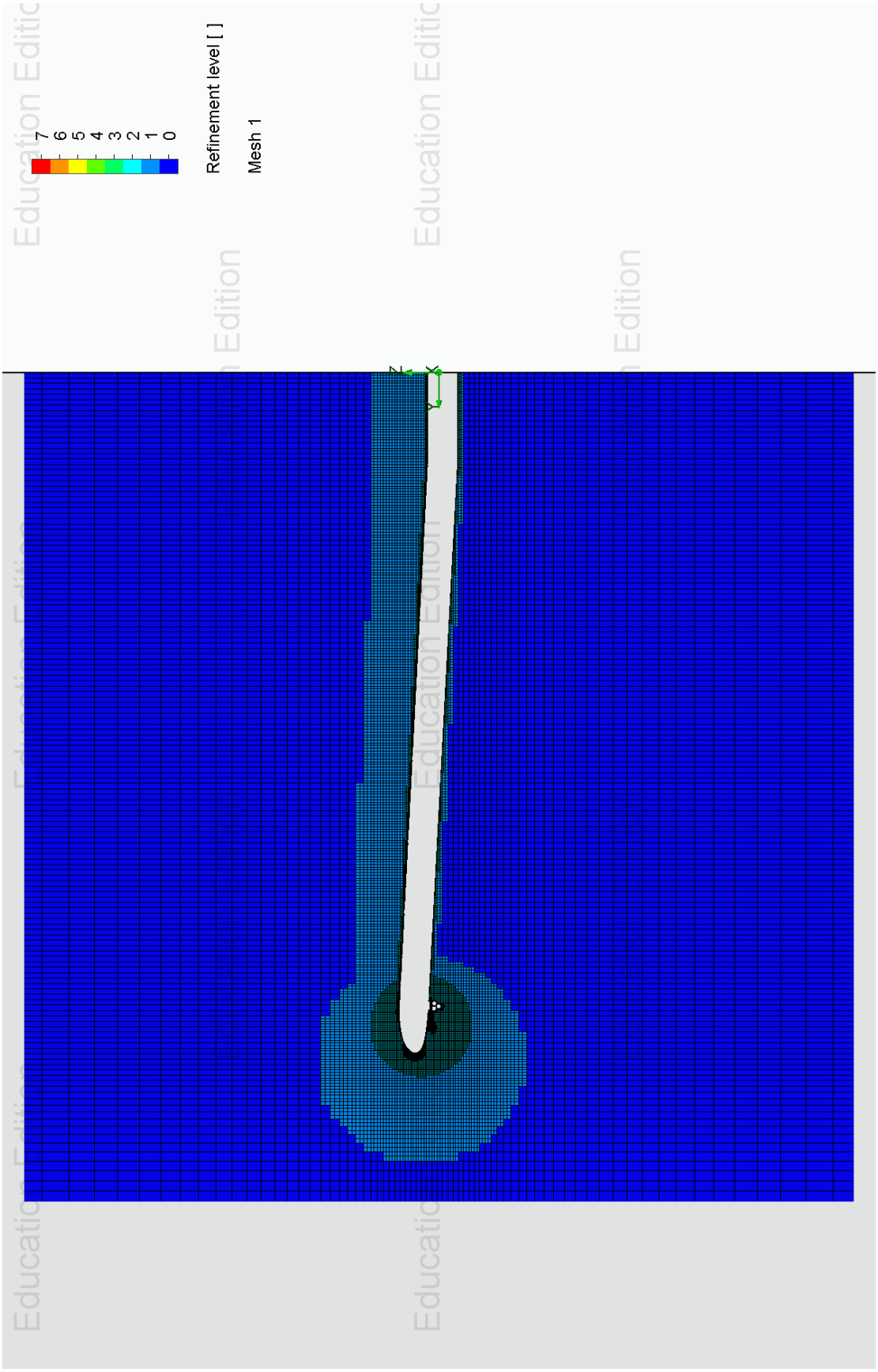

Figure A.9: Mesh for the wing with attachments for case 4.

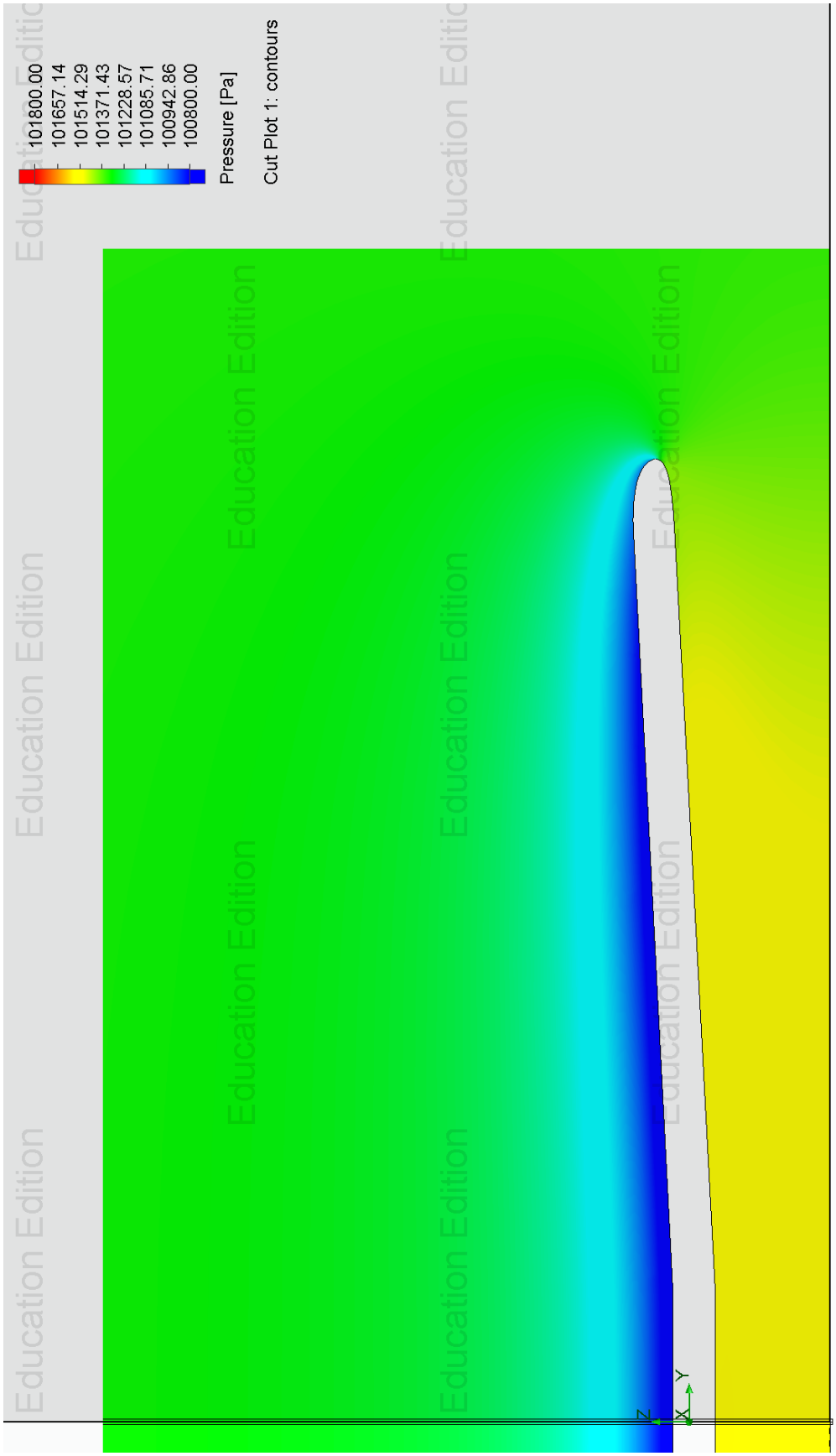

Figure A.10: Pressure contour of the clean wing for case 1.

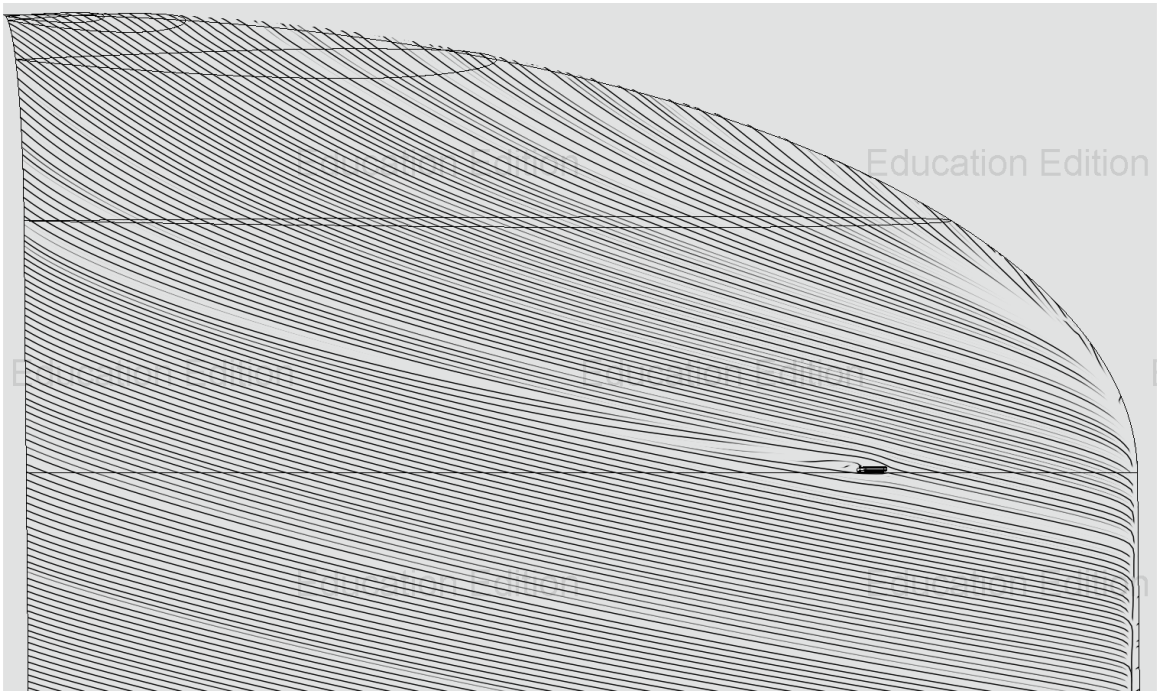

Figure A.11: Streamlines of the clean wing for case 1.

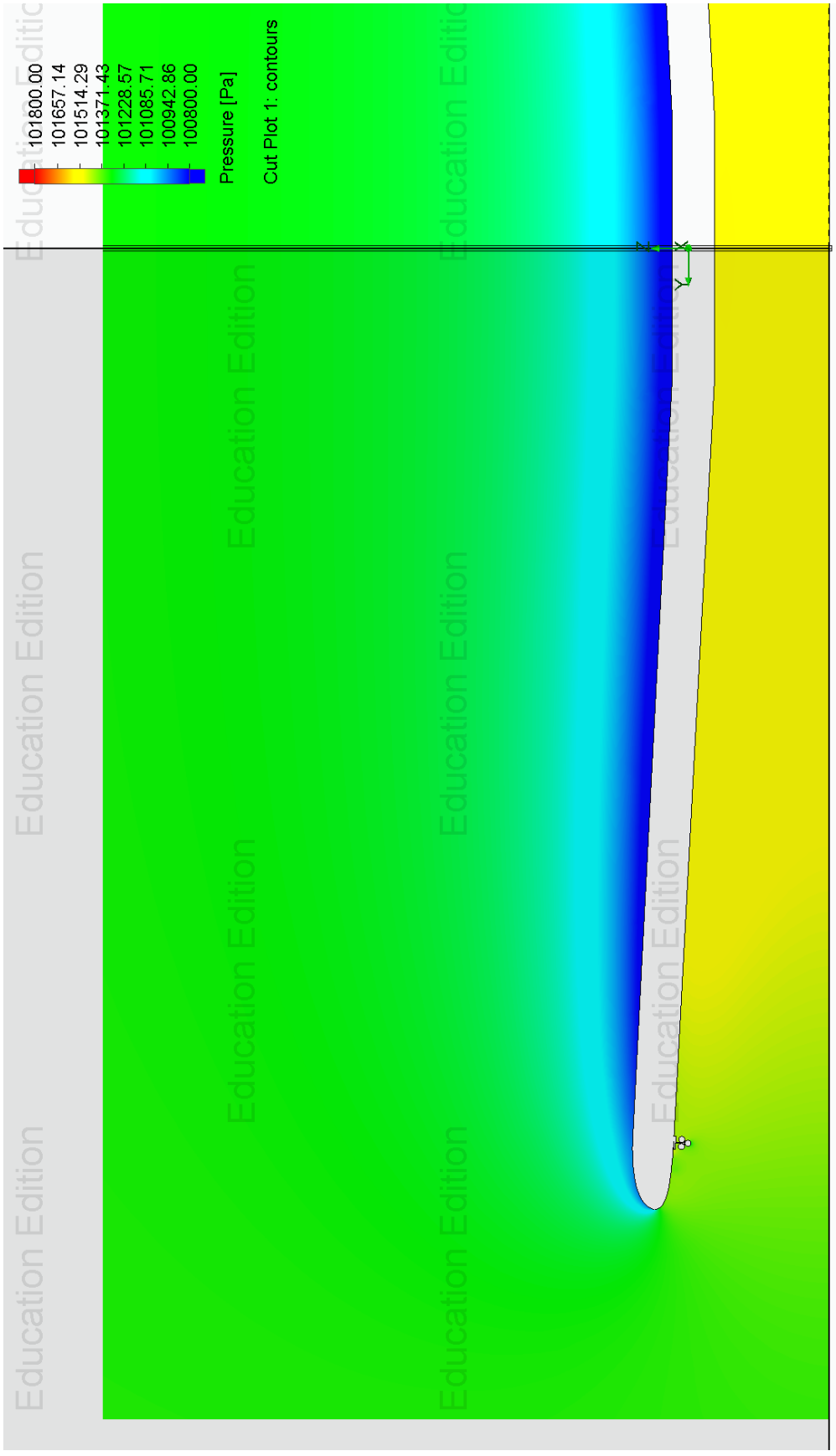

Figure A.12: Pressure contour of the wing with launch platforms for case 2.

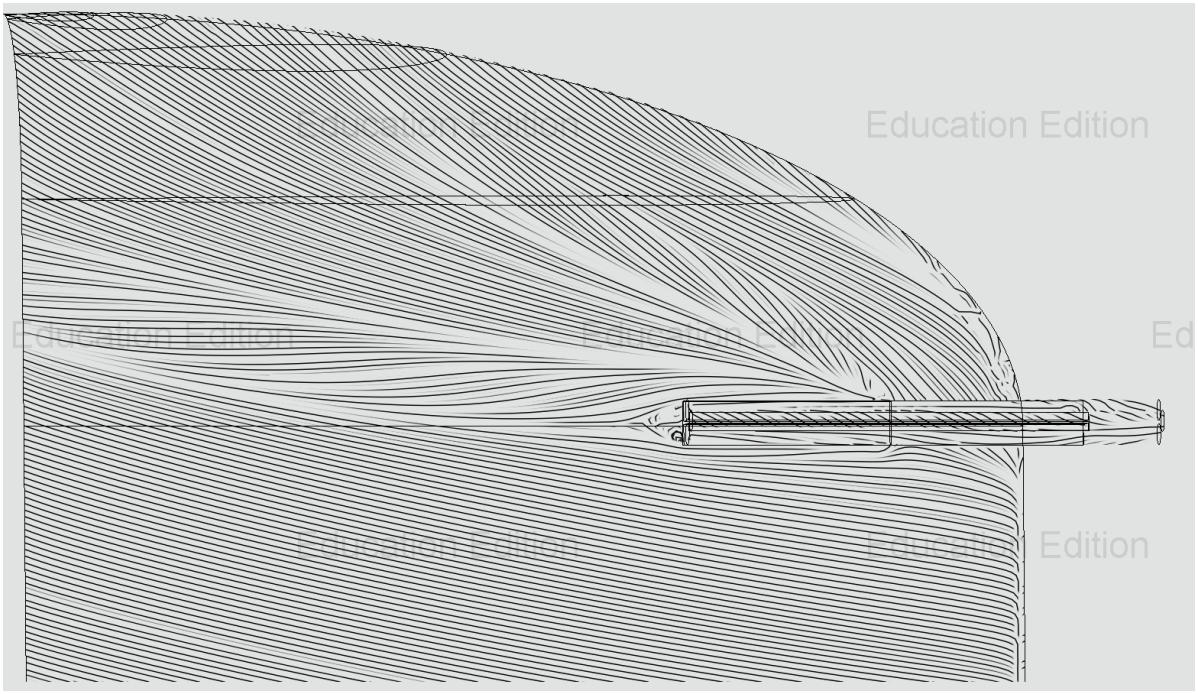

Figure A.13: Streamlines of the wing with launch platforms for case 2.

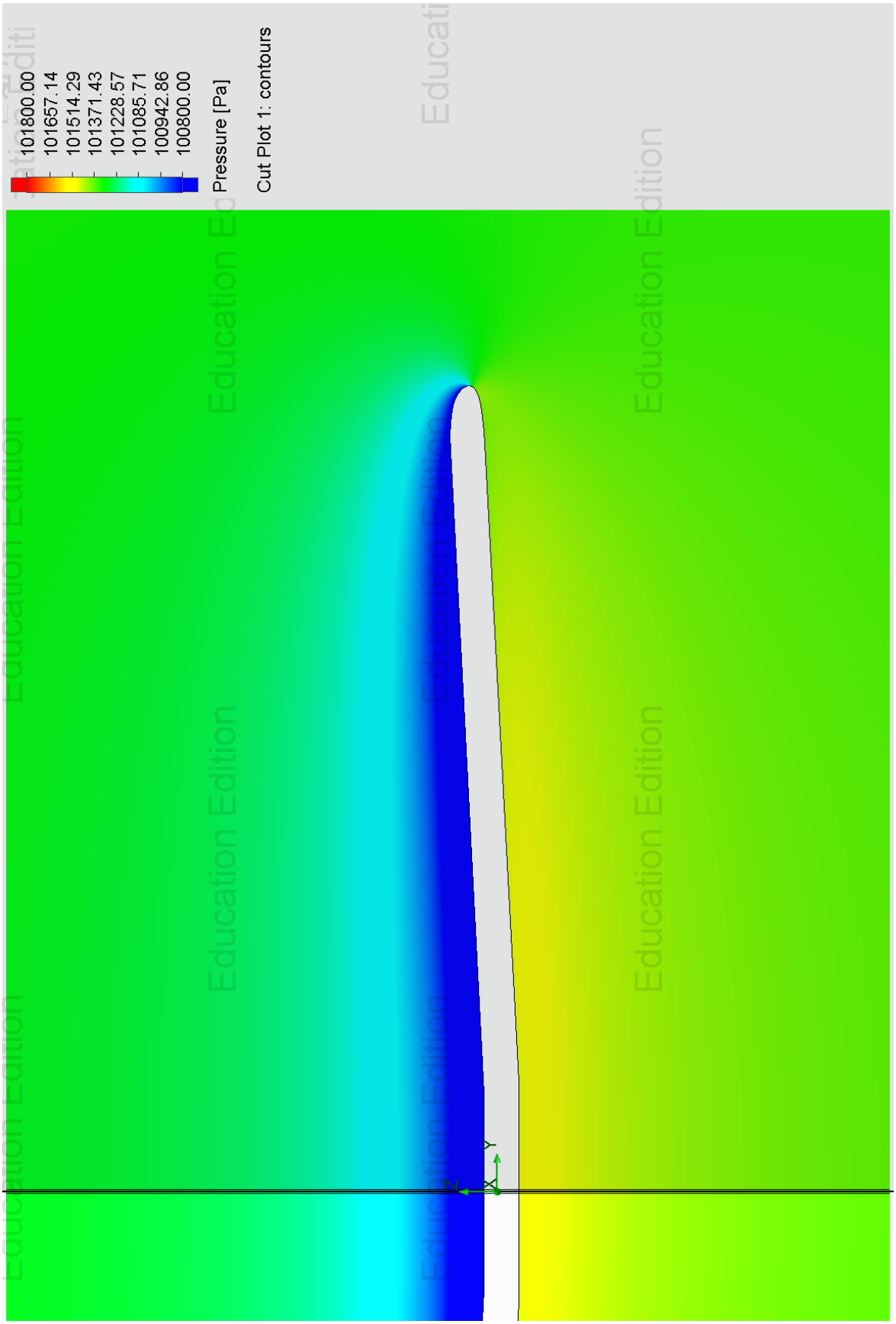

Figure A.14: Pressure contour of the clean wing for case 3.

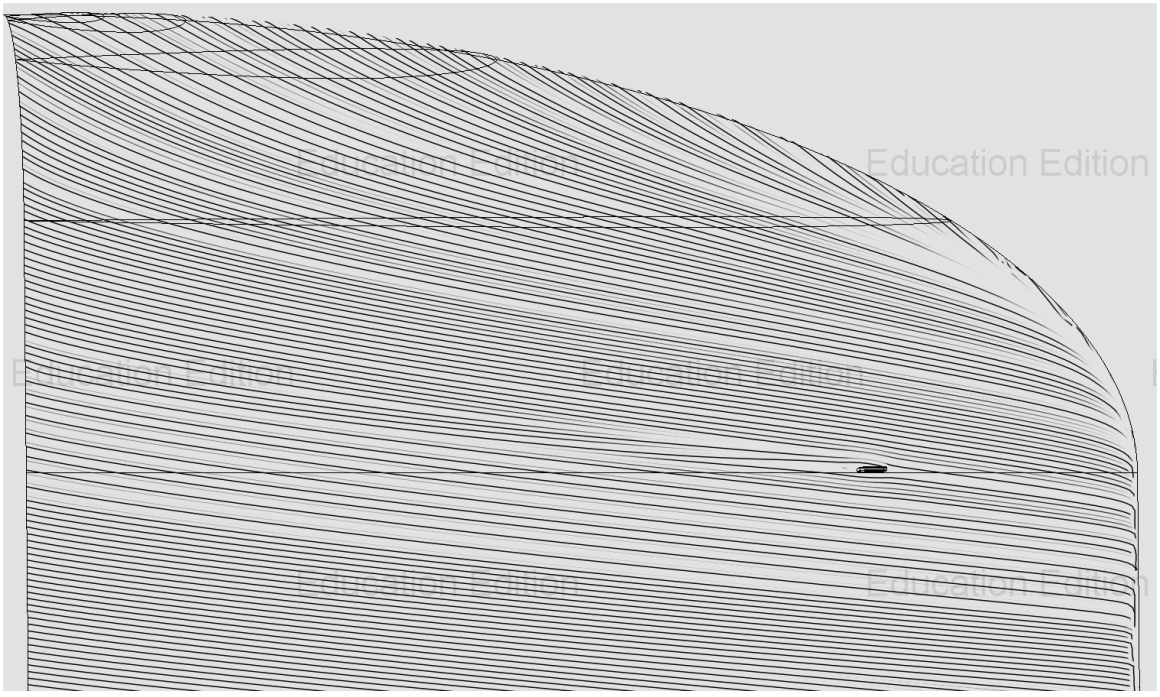

Figure A.15: Streamlines of the clean wing for case 3.

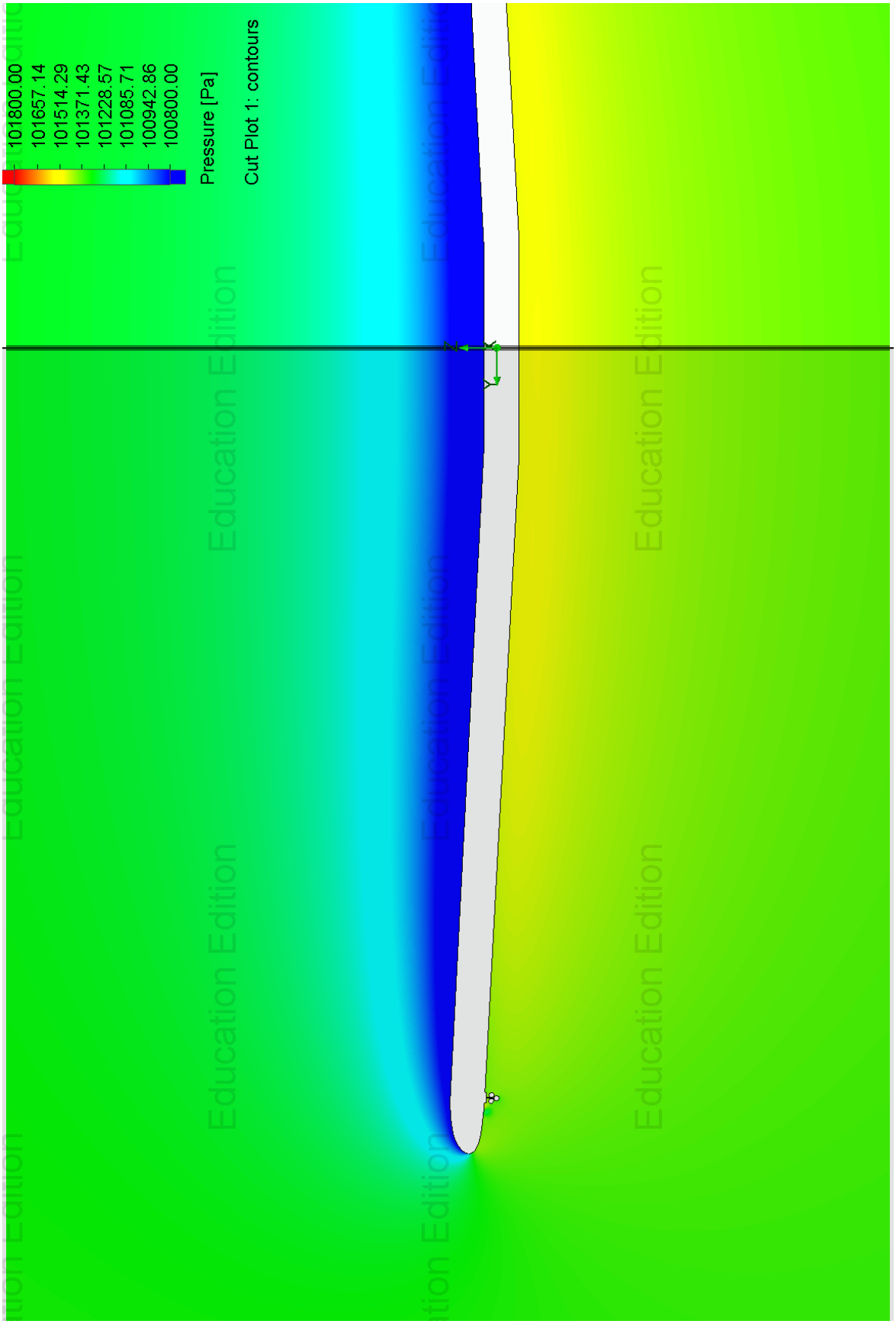

Figure A.16: Pressure contour of the wing with launch platforms for case 4.

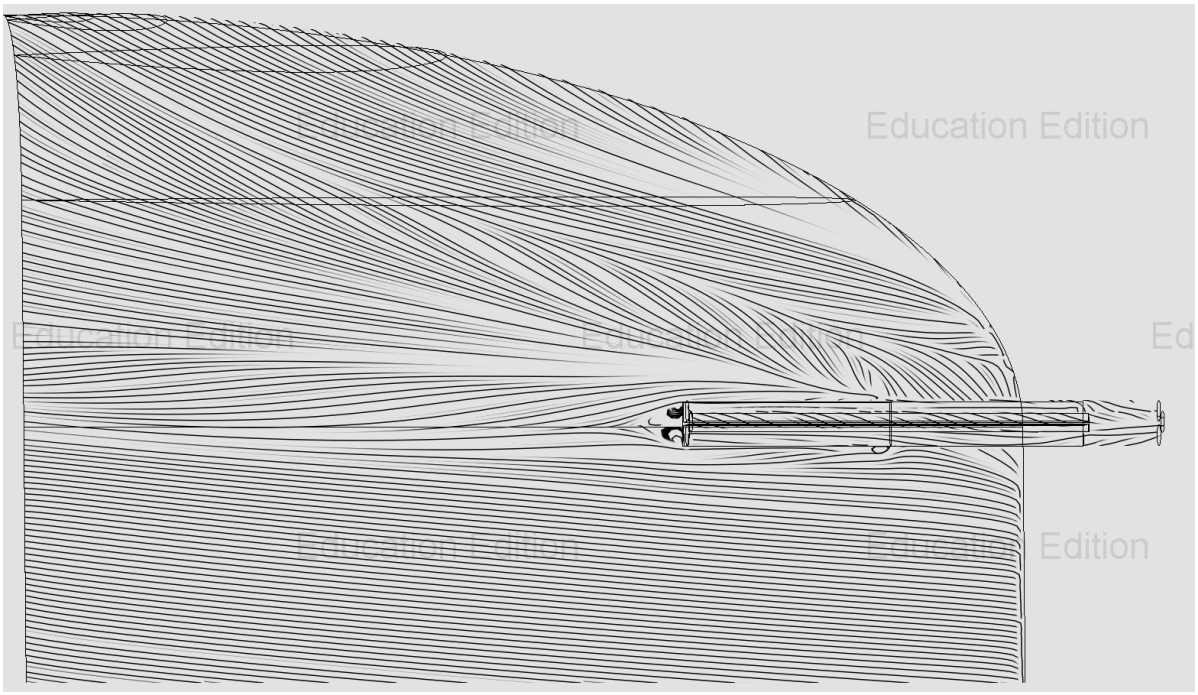

Figure A.17: Streamlines of the wing with launch platforms for case 4.

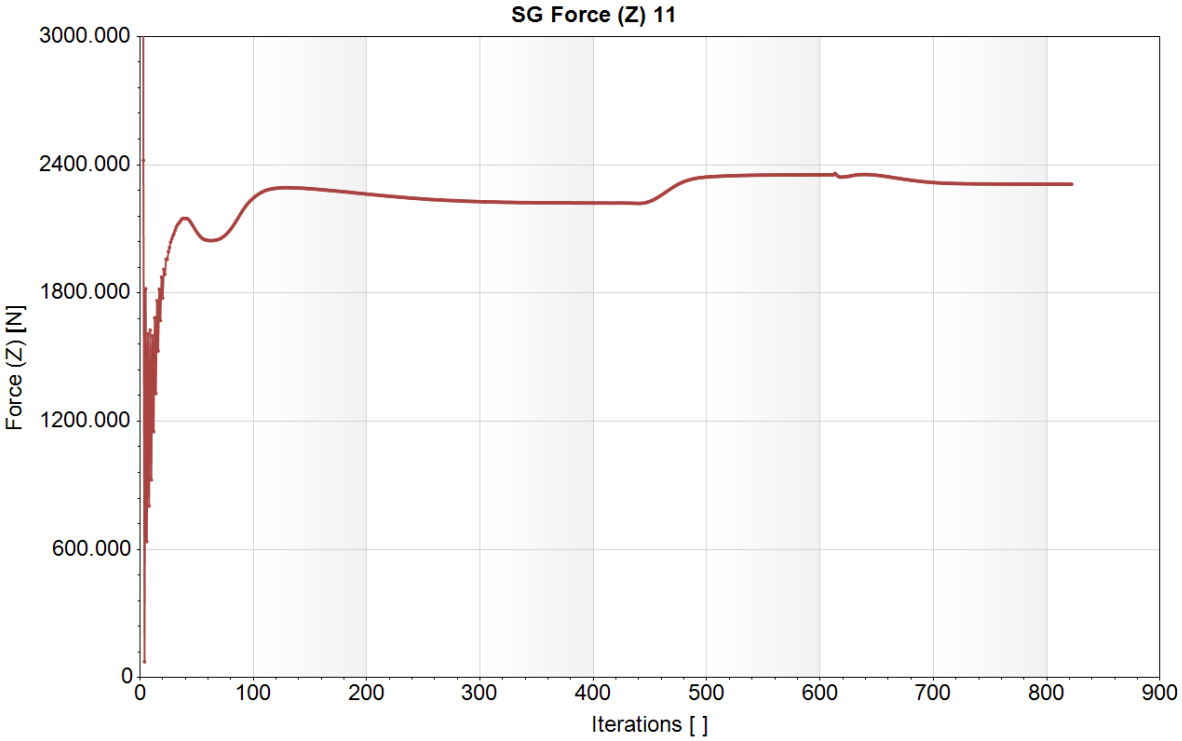

Figure A.18: Convergence of the half wing lift force in Z for the clean wing at take-off.

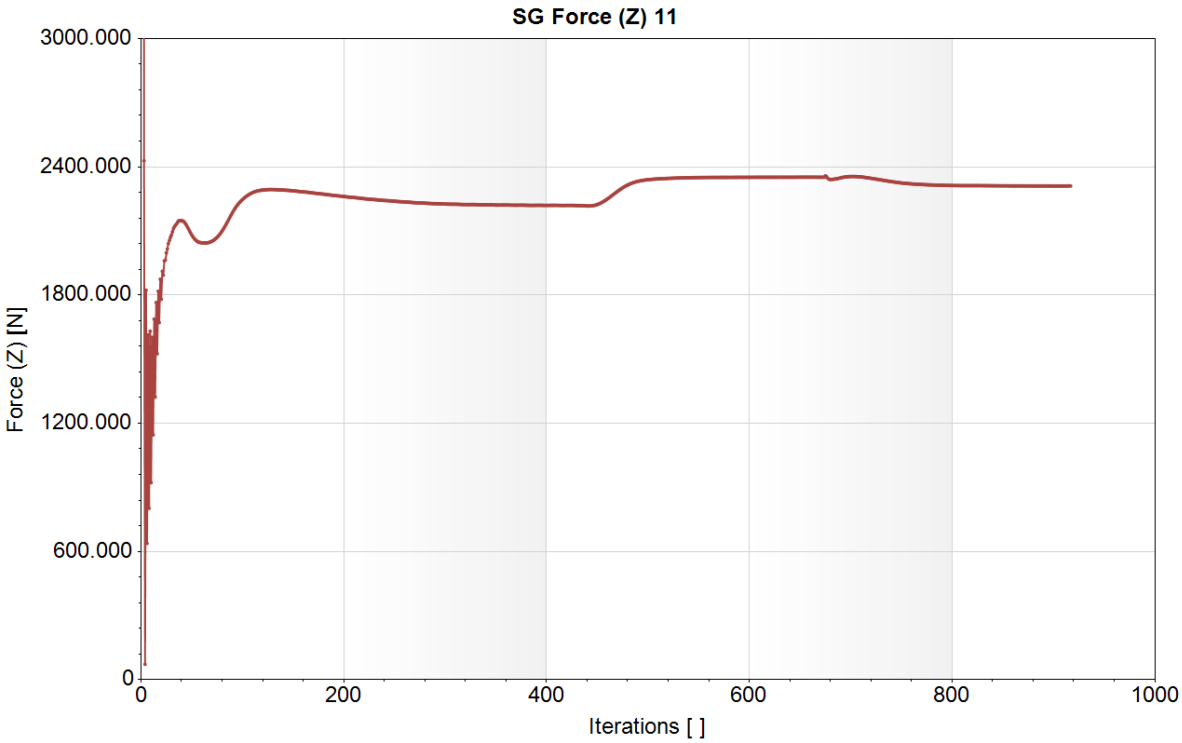

Figure A.19: Convergence of the half wing lift force in Z for the wing with launch platform at take-off.

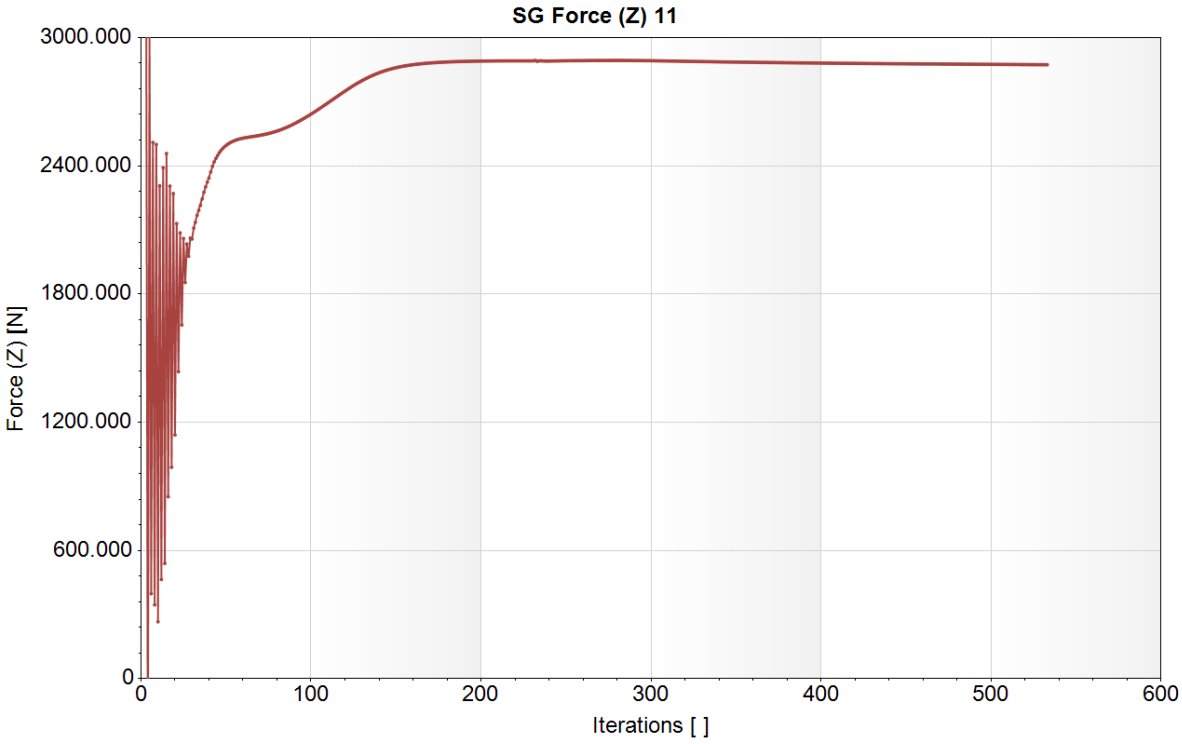

Figure A.20: Convergence of the half wing lift force in Z for the clean wing during steep turn.

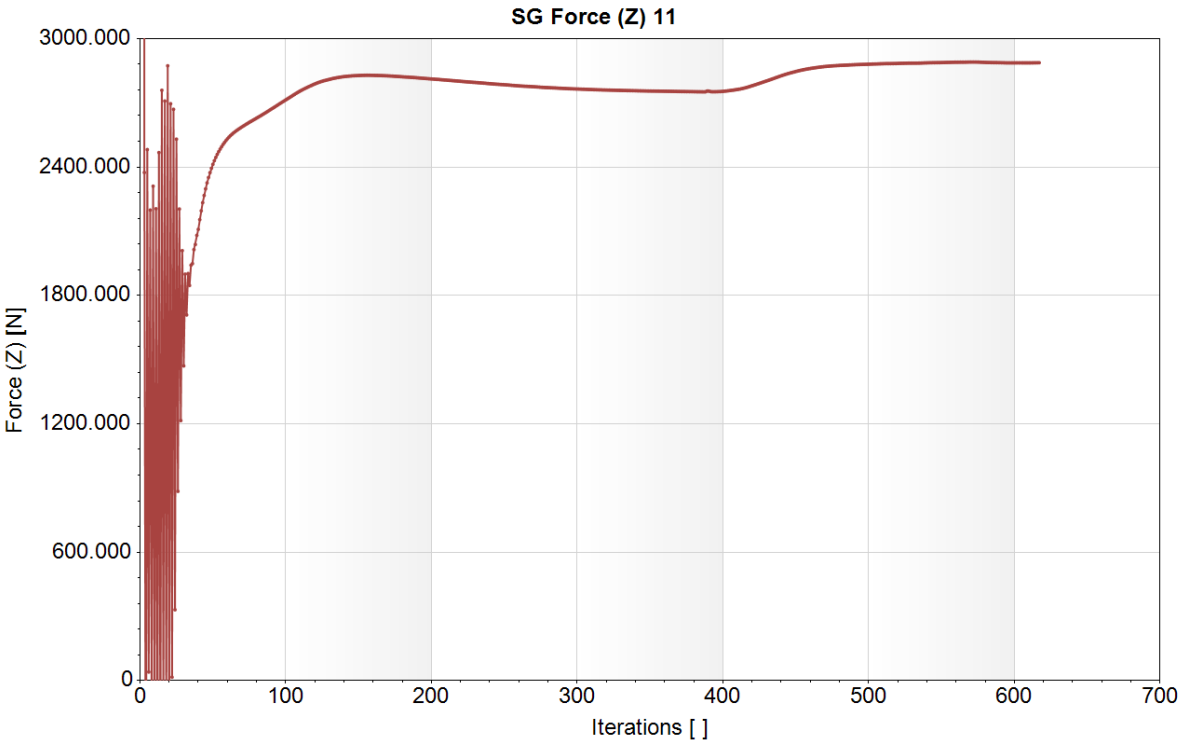

Figure A.21: Convergence of the half wing lift force in Z for the wing with launch platform during steep turn.

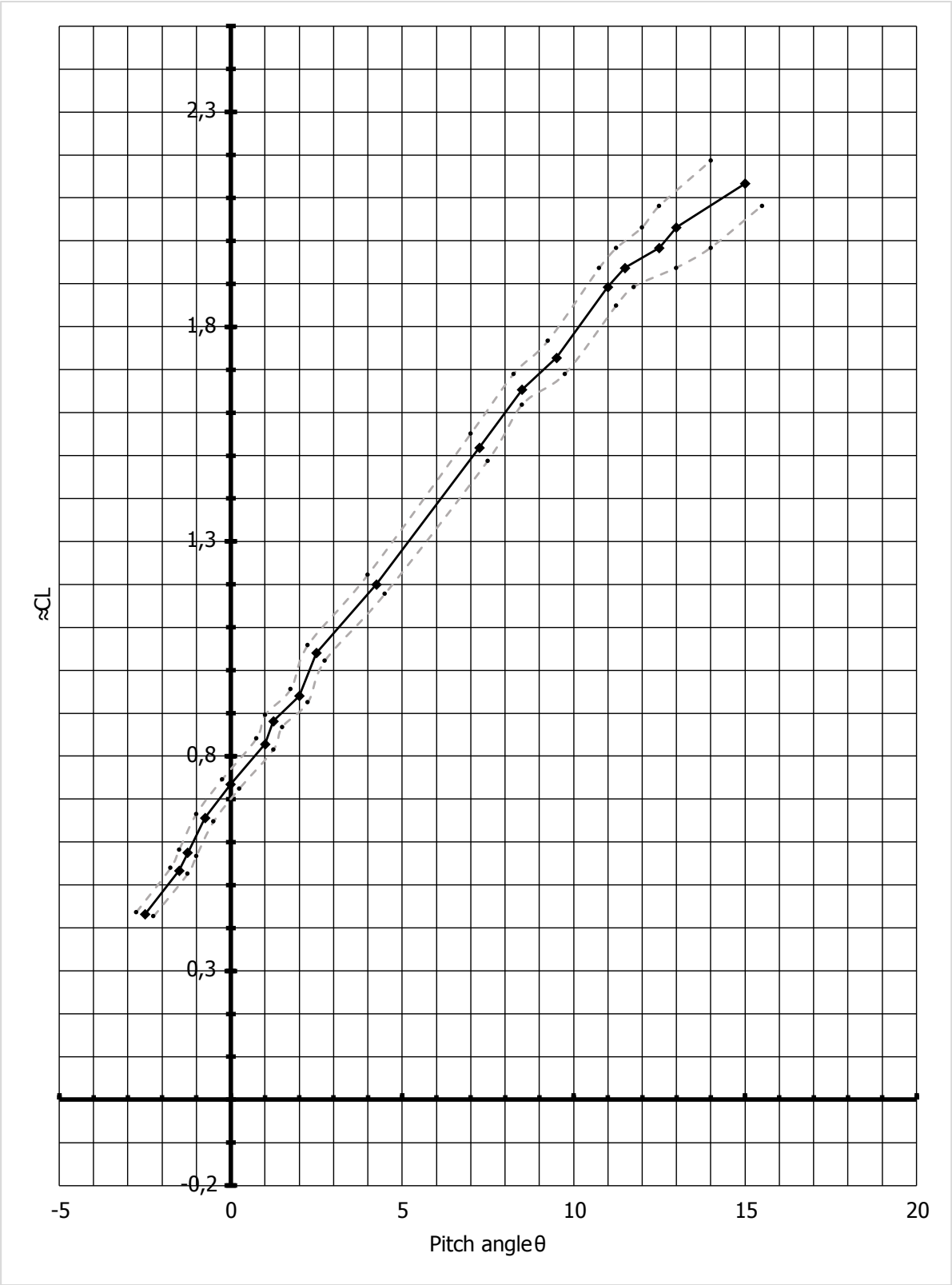

Figure A.22: CL - θ plot of the Evektor Sportstar RTC aircraft
With indication of uncertainty in θ by dot markers

Bibliography

[1] Wikipedia contributors, *Bréguet 14,* (2023), accessed: NA-NA-NA.

[2] Wikipedia contributors, *File:Wing fences on the wing of a caravelle.jpg,* https://en.m.wikipedia.org/wiki/File:Wing_fences_on_the_wing_of_a_Caravelle.jpg (2023), accessed: NA-NA-NA.

[3] E. J. McFadden, P. J. Brandt, and J. P. Bons, *Swept wing active flow control using a streamwise row of vortex generating jets,* in *AIAA SCITECH 2022 Forum* (AIAA, 2022) Chap. 1546, p. 13, https://arc.aiaa.org/doi/pdf/10.2514/6.2022-1546 .

[4] *All sizes,* https://www.flickr.com/photos/a380spotter/14691292545/sizes/l/ (2020), accessed: 2023-9-27.

[5] S. Gudmundsson, *Chapter 23 - miscellaneous design notes,* in *General Aviation Aircraft Design*, edited by S. Gudmundsson (Butterworth-Heinemann, Boston, 2014) pp. 947–983.

[6] D. Scholz, *Definition and discussion of the intrinsic efficiency of winglets,* INCAS BULL. (2023).

[7] *File:Wingtip device on a china eastern airlines airbus a330-343.jpg,* https://commons.wikimedia.org/wiki/File:Wingtip_device_on_a_China_Eastern_Airlines_Airbus_A330-343.jpg (2023), accessed: 2023-10-21.

[8] *File:Wingtip fence airbus A320.JPG,* https://commons.wikimedia.org/wiki/File:Wingtip_Fence_Airbus_A320.JPG (2023), accessed: 2023-10-21.

[9] J. P. Santiago, *The spiroid winglet,* http://aviationtrivia.blogspot.com/2010/08/spiroid-winglet.html (2023), accessed: 2023-10-21.

[10] Laurent, *Spin,* https://www.studyflight.com/spin/ (2017), accessed: 2023-9-27.

[11] https://www.faa.gov/sites/faa.gov/files/13_phak_ch11.pdf (2016), accessed: 2023-9-27.

[12] C. Atlamazoglou, *The US air force is finally getting rid of its a-10s, and its focus may be straying from the warthog's unique mission,* Business Insider (2023).

[13] *No title,* https://twitter.com/AmRaadPSF/status/1622173205187149824/photo/1 (2023), accessed: 2023-10-21.

[14] D. J. J. Davilla and A. Soltan, *French Aircraft of the First World War* (Flying Machines Press, 1997) pp. 88–89.

[15] A. Żyluk, *Experimental validation of mathematical model describing external stores separation,* JOURNAL OF THEORETICAL AND APPLIED MECHANICS **43**, 855 (2005).

[16] C. of Naval Air Training, *T-45 aerodynamics student workbook,* (2009).

[17] H. H. J. Hurt, *Navair 00-80t-80, aerodynamics for naval aviators,* Naval Air Systems Command (1965).

[18] R. L. R. Richard S Shevell, Roger D Schaufele, *Stall control device for swept wings,* (1968).

[19] R. D. Schaufele, *Applied aerodynamics at the douglas aircraft company,* AIAA 99-0118 (1999).

[20] R. D. Schaufele and R. S. Shevell, *Aerodynamic design features of the dc-9.* Journal of Aircraft **3**, 515 (1966).

[21] J. M. McClellan, *Bae 1000 lifts hawker name to new heights,* Flying: 88 (1993).

[22] B. Rutan, *Vortilons for variezes,* The canard pusher (1984).

[23] M. Abzug and E. Larrabee, *Airplane Stability and Control: A History of the Technologies that Made Aviation Possible*, Cambridge Aerospace Series (Cambridge University Press, 2002).

[24] R. T. Whitcomb, *A DESIGN APPROACH AND SELECTED WIND-TUNNEL RESULTS AT HIGH SUB-SONIC SPEEDS FOR WING-TIP MOUNTED WINGLETS*, Tech. Rep. (NASA Langley Research Center, 1976).

[25] D. Gueraiche and S. Popov, *Winglet geometry impact on dlr-f4 aerodynamics and an analysis of a hyperbolic winglet concept,* Aerospace **4**, 60 (2017).

[26] N. E. Haddad, *Aerodynamic and structural design of a winglet for enhanced performance of a business jet,* Dissertations and Theses (2015).

[27] https://cms.education.gov.il/NR/rdonlyres/D9F6FC7B-A508-43C8-BB34-5C6D8AE0346D/178686/Understanding_Winglets_Technology.pdf (2000), accessed: 2023-9-27.

[28] L. Penning, *Boeing designs advanced technology winglet for 737 max,* Boeing (2012).

[29] L. Demasi, G. Monegato, R. Cavallaro, and R. Rybarczyk, *Minimum induced drag conditions for winglets: the best winglet design concept,* in *AIAA Scitech 2019 Forum* (AIAA, 2019) Chap. 2301, p. 48, https://arc.aiaa.org/doi/pdf/10.2514/6.2019-2301 .

[30] *Types of blended winglets,* https://www.aviationpartners.com/aircraft-winglets/types-blended-winglets/ (2016), accessed: 2023-10-21.

[31] Wikipedia contributors, *File:DSC 8030-F-WZGG - MSN 003 (10512622646).jpg,* https://en.m.wikipedia.org/wiki/File:DSC_8030-F-WZGG_-_MSN_003_(10512622646).jpg (2023), accessed: NA-NA-NA.

[32] Z. Najafianashrafi and A. Sedaghat, *Improving the aerodynamic performance of a wing with winglet,* International Journal of Natural and Engineering Sciences **8**, 52 (2014).

[33] E. T. S. William Freitag, *Blended winglets improve performance,* Aeromagazine (2009).

[34] S. Rajendran, *Design of Parametric Winglets and Wing tip devices - A Conceptual Design Approach*, Tech. Rep. (Linkoping University, 2012).

[35] G. Narayan and B. John, *Effect of winglets induced tip vortex structure on the performance of subsonic wings,* Aerospace Science and Technology **58**, 328 (2016).

[36] S. Mostafa, S. Bose, A. Nair, A. Raheem, T. Majeed, A. Mohammed, and Y. Kim, *A parametric investigation of non-circular spiroid winglets,* EPJ Web of Conferences **67** (2014), 10.1051/epjconf/20146702077.

[37] I. Aviation Partners, *Types of blended winglets,* (2023).

[38] A. F. Molland and S. R. Turnock, *3 - physics of control surface operation,* in *Marine Rudders and Control Surfaces*, edited by A. F. Molland and S. R. Turnock (Butterworth-Heinemann, Oxford, 2007) pp. 21–56.

[39] A. Rojewski and J. Bartoszewicz, *Usage of wing in ground effect to maintain lift force with reduced fuel consumption of aircraft,* Combustion Engines **169**, 158 (2017).

[40] W. Buler, L. Loroch, K. Sibilski, and A. Zyluk, *Evaluation and experimental validation of low costs cfd based mathematical model describing external stores separation,* JOURNAL OF THEORETICAL AND APPLIED MECHANICS , 21 (2004).

[41] E. s.r.o., https://www.cycloonholland.nl/wp-content/uploads/2016/09/POH-SportStar-RTC-FIO.pdf (2012), accessed: 2023-9-28.

[42] D. Lednicer, *The incomplete guide to airfoil usage,* https://m-selig.ae.illinois.edu/ads/aircraft.html (2023), accessed: 2023-9-28.

[43] M. Graphics, *Floefd aerospace validation and test-cases,* (2010).

[44] *Simcenter FLOEFD: CFD for designers and engineers alike – part 1,* https://bsim-engineering.com/simcenter-floefd-cfd-for-designers-and-engineers-alike-part-1/?lang=en (2020), accessed: 2023-10-21.

[45] P. A. . Ul, a. . Ul, h. . Ul, h. . Ul, U. L. /avgas, and P. . Of, *Safety data sheet,* https://www.hjelmco.com/upl/files/151908.pdf (2023), accessed: 2023-9-29.

[46] A. Ulazia, A. Nafarrate, G. Ibarra-Berastegi, J. Sáenz, and S. Carreno-Madinabeitia, *The consequences of air density variations over northeastern scotland for offshore wind energy potential,* Energies **12** (2019), 10.3390/en12132635.

[47] Wikipedia contributors, *Dew point — Wikipedia, the free encyclopedia,* https://en.wikipedia.org/w/index.php?title=Dew_point&oldid=1175435733 (2023), [Online; accessed 29-September-2023].

[48] G. Ballester, *Formulario para peticion de mensajes aeronauticos,* https://www.ogimet.com/metars.phtml.en (2023), accessed: 2023-10-4.

[49] *Sample size calculation and sample size justification,* https://www.statisticssolutions.com/dissertation-resources/sample-size-calculation-and-sample-size-justification/ (2010), accessed: 2023-11-23.